Hybrid Inorganic/Organic Infrared Imaging Upconversion Devices

by

Mark Ferguson

A thesis

presented to the University of Waterloo

in fulfillment of the

thesis requirement for the degree of

Master of Applied Science

in

Electrical and Computer Engineering

Waterloo, Ontario, Canada, 2015

I hereby declare that I am the sole author of this thesis. This is a true copy of the thesis, including any required final revisions, as accepted by my examiners.

I understand that my thesis may be made electronically available to the public.

Abstract

Upconversion of near-infrared to visible light in a single, hybrid organic/inorganic device is explored in the following work. The components of the photodetector and organic light emitting diode, and the challenge of combining them into a functional system without compromising either significantly, are discussed in theory, the work of previous researchers, and in results presented here for the first time. The large number of interfaces and the large diversity of conceivable parts, and the variety of treatments which may make components more or less compatible, opens up a large territory of upconverter devices which this thesis addresses in a straightforward manner, with minimally-complex (first-generation) devices.

Complications in the assembly of high-efficiency and high-fidelity upconversion devices are described quantitatively from the experimental results, and performance issues are sourced to particular regions and fabrication steps to recommend future iterations of research for improved devices.

Acknowledgements

I would like to thank my supervisor, Professor Dayan Ban, for his persistent guidance in my research. I would also like to thank my co-supervisor, Professor Hany Aziz, for his helpful advice, and for inviting me into his group of passionate organic electronics researchers.

I am furthermore indebted to Richard Barber and Robert Mullin for their daily labours in making the Giga-to-Nano Centre a productive and enjoyable research facility. My fellow G2n researchers have also been essential for their assistance in first training me as a new member on many pieces of equipment, and then cooperating in the sharing of precious lab resources. Special thanks in particular go to Graeme Williams, Jian Zhang and Mike Zhang.

In my other lab work I must thank Ghasem Razavi, Rudra Dhar, Guocheng Liu, Chao Xu, Simon Ferre and Nolan Lassaline for their regular assistance.

I do not know if developing higher technology for humans does any good for our longevity as a species, but in my own life I consider it fun to watch both the use and the misuse. This thesis is dedicated, like everything I write, to whatever future humans there will be left to read it.

Table of Contents

List of Figures

List of Tables

List of Abbreviations

Alq_3: Tris(8-hydroxyquinolinato) aluminium

BHF: Buffered hydrogen fluoride

CCD: Charged-Coupled Device

CuPc: Copper phthalocyanine

EL: Electroluminescent layer

ETL: Electron transport layer

FPA: Focal plane array

HIL: Hole injection layer

HTL: Hole transport layer

Irppy: tris(2-phenylpyrridine) iridium

MBE: Molecular beam epitaxy

NIR: Near infrared

NPB: 1,4-bis(1-naphthylphenylamino)biphenyl

OLED: Organic light emitting diode

PECVD: Plasma enhanced chemical vapor deposition

QWIP: Quantum well infrared photodetector

RIE: Reactive ion etch

RHEED: Reflection high energy electron diffraction

ROIC: Read out integrated circuit

TMAH: Tetramethylammonium hydroxide

TPBi: 1,3,5-tris(N-phenylbenzimidizol-2-yl)benzene

Chapter 1

1.0 Introduction

Sensitive only to wavelengths ranging from 390 to 750 nm, human vision captures a mere slit in the electromagnetic spectrum. Outside those few hundred nanometers are vast orders of magnitude, with wavelengths scrunched to tens of nanometers as ultraviolet radiation, compressed further to Ångstroms as X-ray radiation, but also stretched to microns as infrared radiation, to centimeters as microwave radiation, and to kilometers as radio waves. Scaled logarithmically, humanity's restriction to the visible spectrum is as debilitating a handicap as a mask with a long pipe at its front forbidding sight beyond a 10 degree wedge. Until very recently we have been unable to rotate our head or make the wedge any larger, and we have been blind to whatever might be happening in those other directions.

The ability to see more is often the catalyst for a host of discoveries: detection of X-rays accompanied the first hints of radioactivity; ultraviolet 'black lights' brought fluorescence to human attention; microwave radiation has been detected to confirm and improve theories on the behaviour of the early universe; radar has been used to accurately map the bottom of the oceans and the surface of the Moon. The detection of infrared radiation for a large host of applications – scientific, industrial, medical and military – is the focus of this thesis. Infrared radiation is generally defined as possessing wavelengths ranging from 750 nm to 1 mm. Further divisions are often specified in research, and will be used here: near infrared (750 nm to 3 microns); mid infrared (3-50 microns); and far infrared (50 microns to 1 millimeter).

Ultraviolet and more energetic radiation is effectively screened from conventional human experience by the Earth's atmosphere, but infrared and longer wavelengths are able to penetrate

to the ground level. Some amount of infrared is furthermore emitted by any object above absolute zero. The technology to detect these waves and extract information from them is not without biological precedent: shifting sensitivity to a different spectral range can permit hunting at night, allowing pit vipers and vampire bats to locate mammalian prey. In human hands infrared sensors may be put to use in detecting enemy combatants for a military operation or locating stowaways for border security; thermography of vital equipment in a factory can monitor surfaces for abnormal changes in temperature as early signs of problems, including particularly sensitive industrial processes such as the growth of semiconductor wafer crystals; many objects in space, especially the potentially-hazardous Near Earth Objects, are known only by their slight infrared emissions[1].

1.1 Background

The tracking of any temperature-dependent phenomenon can in principle be used to detect infrared radiation. Pit vipers and vampire bats have evolved temperature-sensitive ion channels in their cellular membranes, along with sophisticated vasculature to cool and zero their detectors to prevent prolonged afterimages[2]. A change in electrical resistivity in response to heat is the operating mechanism of bolometers, which are amongst the most sensitive detectors available in the far infrared. Thermocouples operate by exploiting the Seebeck effect to detect a change in temperature. The pyroelectric response of a few materials is the usual operating mechanism at work in the passive infrared sensors found in burglar alarms and automatic lighting systems. All of these strategies, relying on a temperature change as a consequence of infrared exposure, are termed thermal infrared detectors.

Waiting for a change in temperature may incur an unacceptable delay, however, and this thesis is focused on photonic infrared detectors which register the presence of infrared photons directly. In addition to a more immediate response photonic detection offers far greater sensitivity, conceivably down to the level of a single photon. Extreme sensitivity in detectors presents an issue, however: photonic infrared detectors will be bombarded by the infrared radiation emitted by all objects above absolute zero, including the background environment in addition to the target, resulting in high noise. Consequently, photonic detection must sometimes be done at cool, often cryogenic temperatures, and it is understandable that the technology was originally advanced with great focus on space-based surveillance during the Cold War[3].

1.2 Infrared Detection Materials

The common feature to virtually all photonic infrared detectors is a semiconductor with a suitably small energy band gap. Table 1.2.0 presents the common candidates.

Semiconductor	Band Gap (eV)	Cut-off wavelength (microns)
GaSb	0.68	1.71
GaAs	1.43	0.87
InAs	0.36	3.45
InSb	0.17	7.31
InP	1.27	0.92
CdTe	1.44	0.83

Table 1.2.0: Semiconductor materials of interest to photonic infrared detection, with energy band gaps and cut-off wavelengths[4].

In designing photonic infrared detectors, however, much more must be considered than the energy band gaps of the detector materials. Lattice parameters regulate what films can be conveniently grown in contact with each other to a reasonable thickness, and so over years of

research particular material systems of alloys have been identified as satisfying the lattice constraints while absorbing photons of the desired energy, beginning with the variable band gap HgCdTe ternary alloy discovered by Lawson et al. in 1959[3]. In modern times the indium gallium arsenide system, $In_xGa_{1-x}As$, is particularly well-understood. The selection of an appropriate fraction x permits lattice matching to substrates of germanium ($x = 0.015$) or indium phosphide ($x = 0.53$), each a direct semiconductor of interest in optoelectronic applications. Interpolated mechanical, electrical and optical properties between those of InAs and GaAs have been firmly established by experiment. A satisfying match to an InP substrate produces InGaAs with a cut-off wavelength of 1.68 microns at room temperature, relevant to the detection of near infrared light. The InGaAs system will be central to devices presented in this thesis.

Photonic infrared detectors of this type were developed by Pearsall and Hopson in 1977[5], and competed favorably with equivalent Ge devices within a wavelength range of 1 to 1.6 microns: faster response, greater quantum efficiency, and reduced dark current were demonstrated[6]. When interested in detecting the binary presence or absence of near infrared radiation, particularly between wavelengths of 700 nm to 2.6 microns, such InGaAs photodetectors remain the primary technology of choice. However, constructing an actual image from infrared radiation is an endeavour complex beyond this most fundamental unit, just as a retinal cell is an essential but only preliminary part of an eye.

1.3 Photodetector devices

1.3.1 PN, PIN photodetectors

Apart from photomultipliers, the most primitive form of photonic infrared detector is the PN junction device. When an LED is reverse-biased it can work as a photodiode to absorb light at wavelengths matching or shorter than the LED's emission wavelength; the photons of sufficient energy will create excitons in the depletion region of the PN junction, yielding a current in response to exposure by light. However, PN junctions have incredibly poor performance in isolation due to the small volume of the depletion region between the p- and n-doped layers, as only photons absorbed in this limited volume will generate excitons which will be separated into holes and electrons by the device's intrinsic field to participate in the current; other photons absorbed elsewhere are lost. A PIN-based photodetector introduces a middle layer and a larger volume in which photon absorption can produce useful excitons[7].

This adsorption problem is particularly relevant for long wavelengths of light, particularly the infrared, as they can penetrate deeper into most substrates and are so inclined to be wasted out the back of the photodetector (prompting consideration of mirrors by some researchers). A thick intrinsic layer in a PIN device captures more excitons from absorbed photons, an important advancement upon equivalent PN devices, but the layer thickness must be limited to avoid the necessity of a prohibitively high reverse bias, for across a larger area the intrinsic electric field gradient (dE/dx) will be reduced, and so more excitons will be lost to electron-hole recombination before they can be swept apart to constitute the photocurrent, counteracting the larger number of initial excitons produced in the relevant volume of the device. Carriers also have a limited lifetime, and traversing a greater distance ensures that more will be

lost to recombination even after separation from the exciton state. Furthermore, a sufficiently high reverse bias will also achieve breakdown of the photodetector.

Additional modifications to PN- and PIN-based photodetectors have been developed for specialized circumstances. Avalanche photodiodes can amplify the photocurrents beyond the initial carriers yielded up by the excitons from absorbed photons by bearing a region with a high field gradient, permitting rapidly-moving carriers to collide with and free bound electrons[7]. The high voltages necessary to instigate the avalanche multiplication make these devices limited in application, and the probabilistic nature of carrier collision introduces an additional noise in such detectors. Quieter PIN devices, consuming less power, will be without such modification, and so it will be practical to introduce an electrical gain in photocurrent by considering a more complicated design: the heterojunction phototransistor.

1.3.2 HPT photodetectors

Heterojunction phototransistors are essentially bipolar transistors, bearing base, collector and emitter layers and two PN junctions. Excitons form in the base-collection region due to photon absorption, and carriers are injected into the base and amplified by the participation of thermally-generated carriers moving from the emitter into the base by diffusion. As with PN and PIN devices carrier recombination limits the thickness of the absorbing layer (the HPT's base), to ensure that carriers traverse the region within the minority carrier's lifetime. The ratio of carriers injected from the emitter to the collector to the electrons injected from the base is the critical value that determines the current gain of the HPT. By consuming electrical power the HPT can inject multiple carriers in response to a single photon of infrared light, yielding a larger photocurrent[7].

An important limitation affecting HPT devices, besides the greater complexity of their fabrication, is the delay their signals incur due to internal capacitances between the device layers. These delays (on the scale of microseconds) are particularly handicapping for the high-speed detection of light, and would limit the practicality of HPTs in applications involving data transmission, but they are not relevant for this project. Table 1.3.0 displays the layer structure of a pnp-doped HPT wafer, the starting point for fabrication into an HPT photodetector, grown by Molecular Beam Epitaxy (see Chapter 2).

Material (dopant)	**Thickness (nm)**
InGaAs (Zn)	500
InGaAs (Zn)	1000
InGaAs (Si)	60
InGaAs (undoped)	10
InP (Zn)	100
InP (Zn)	500

Table 1.3.0: A pnp-HPT layer structure.

1.3.3 Quantum Well photodetectors

Quantum well infrared photodetector (QWIP) devices introduce the powerful advantage of being responsive to a wide range of infrared emission. They bear a series of quantum wells, containing up to hundreds of wells, with a precise thickness and doping of layers ensuring a precise energy gap size in the wells. When the device is biased electrons can be excited from the wells by absorption of infrared light, with the cut-off wavelength of the photodetector being precisely tunable[8]. Many applications take interest in multi-spectral analysis of infrared light, as a target can be separated from a background by pinpointing wavelengths of maximum contrast. Their great handicap, however, is a dependence on cryogenic conditions to operate with reasonable

efficiency; additionally, they are sensitive to the ambient infrared light released by all objects above absolute zero.

Fabrication of QWIP devices is also significantly more complex than fabrication of PN, PIN and HPT photodetectors; the multiple quantum wells, especially hundreds of wells, demand a sophisticated wafer growth process. Simulation of these devices to design the appropriate layer thicknesses, doping concentrations and doping profiles is also a very arduous task, risking inaccuracies when the actual device is fabricated and tested.

1.4 Focal Plane Arrays

Silicon persists as the most developed semiconductor substrate at the time of writing, a popularity fueled by acceptable physical properties and economic convenience. For optoelectronic applications silicon is quite inadequate, however, as it is an indirect semiconductor with low rates of adsorption and recombination. Consequently, it is difficult for optoelectronic engineers to make direct use of the advances made in silicon crystal growth and micro- and nano-fabrication, or use of the sophisticated silicon-based integrated circuits adept at processing the data needed to create real-time images. An interface between direct semiconductors such as Ge, GaAs, InP or InGaAs and Si must be carefully designed and fabricated, and the final product will be a two-layer imaging system: the Focal Plane Array.

The state-of-the-art technique for creating an interface between infrared detectors and silicon read-out integrated circuits (ROICs) is indium bump bonding[9]. After the photodetector components have been fabricated pillars of In are created on the surface, and the ROIC is aligned and bonded to the photodetector substrate by compression, with heating occasionally being necessary. These extra steps, particularly the compression of the photodetector substrate to

ensure firm electrical contact, may deform or misalign critical features. As a further handicap, the bonded features in the FPA are now stuck between the two substrates, inaccessible for future processing or correction. Figure 1.4.0 shows the general FPA setup.

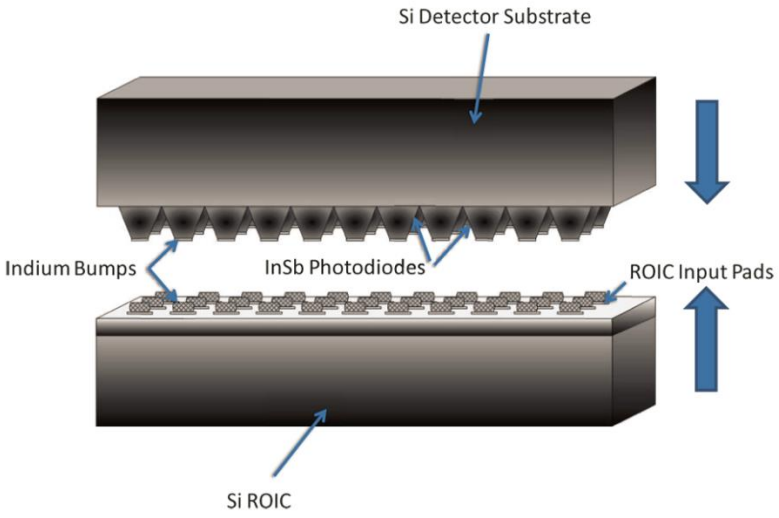

Figure 1.4.0: Typical focal plane array setup[9], with two wafers aligned and bonded together with indium bumps. Ensuring good electrical contact between photodetectors and the read out integrated circuit demands applying heat and pressure, compromising the array's uniformity.

In an ideal FPA each photodetector element would produce the same electrical response to the same input of infrared light. The application of heat and pressure across the entire array makes this practically unattainable, and it is necessary to calibrate the array's responses to standardized infrared input to generate a meaningful detector. Further computational work must be done to convert the analogue signals from the detectors into a digital output which can be presented on a screen. Thus, the photodetectors must be accompanied by a great amount of extra hardware, analogous to the considerable amount of neural circuitry needed to produce vision from the input of retinal cells.

1.5 Upconverters

An alternative to two In-bonded surfaces in a FPA is a single device called an upconverter, and this thesis is dedicated to the demonstration of components in a near-infrared-to-visible-light (NIR) upconverter device which can be created on a single substrate, abstaining from the complications of an electrical interface between two substrates and the subsequent computational corrections needed in contemporary infrared imaging. Figure 1.5.0 presents the general setup of an upconverter device[10], which produces a visible light image from a NIR source to be captured by a CCD (Charged-Coupled Device) camera, in contrast to the contemporary FPA.

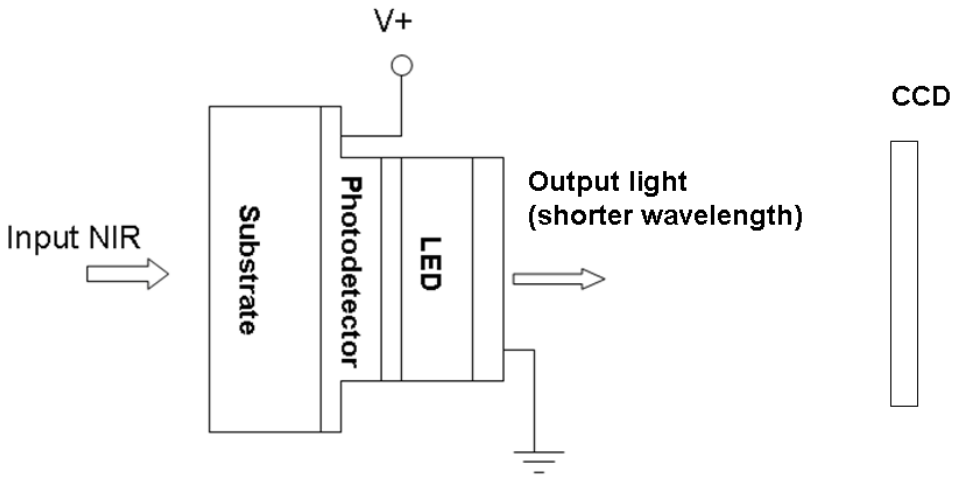

Figure 1.5.0: Generic upconverter device schematic. The visible output is recorded by a CCD camera[10].

Linear upconverters generate output light of a higher energy than the input light by consuming electrical power. Alternative designs, emitting one higher-energy photon in response to the absorption of multiple lower-energy photons, are founded on nonlinear optical materials undergoing such phenomena as second harmonic generation, as occurs to produce the green light of common laser pointers from an infrared source, but these upconverters are more challenging

to model and fabricate, and they operate in a regime of high intensity which is generally impractical for many infrared applications[11]. In linear NIR upconversion a photodetector element generates a photocurrent and transmits charges directly into a light emitting diode (LED) above the photodetector.

A NIR upconverter of this type was first demonstrated by Liu et al. in 1995[12]. This design bore a quantum well infrared photodetector (QWIP) as the detector element, founded on the AlGaAs system, set underneath a conventional LED founded on the InGaAs system, as shown in Figure 1.5.1.

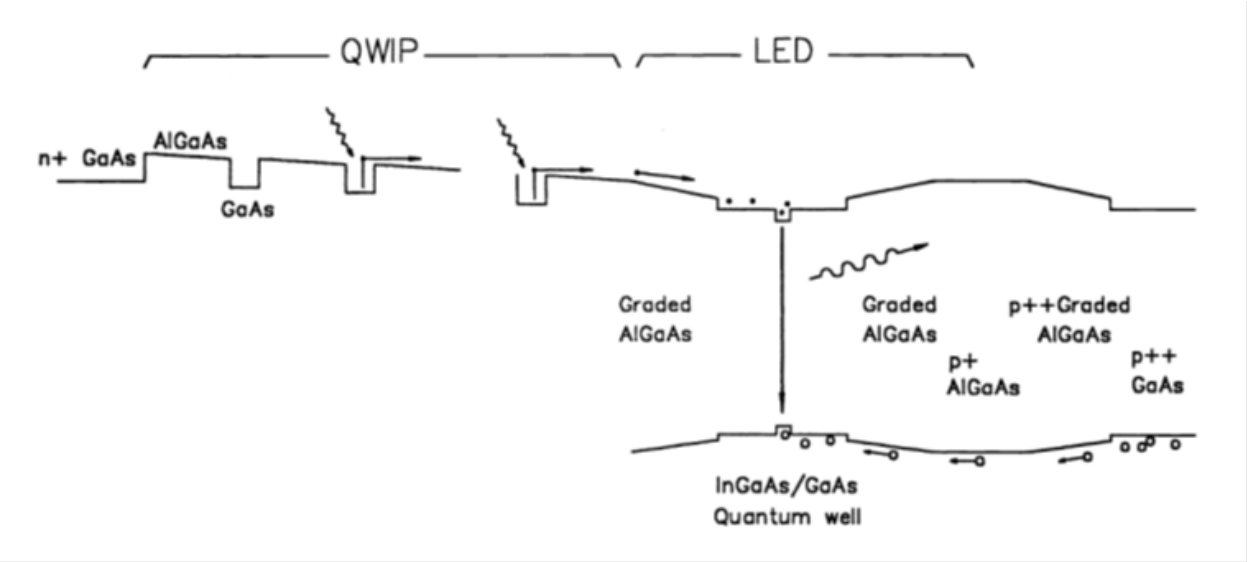

Figure 1.5.1: NIR-to-visible upconversion device developed by Liu et al.[12]. Infrared adsorption in the QWIP layers liberates electrons which are injected into the LED, combining in another quantum well to release visible light.

This particular device, due to the choice of a QWIP, was capable of response to middle and far infrared input as well, but was heavily dependent on cryogenic conditions, demonstrating efficiencies ~300 times greater at 77 K than at room temperature. The actual upconversion

efficiency, comparing watts of input and output light, was a mere 0.8 percent. These first-generation problems were largely blamed on low extraction efficiency of the LED, combined with a large refractive-index mismatch at the air/LED interface.

1.6 Wafer Bonding

One significant constraint in Liu's design and similar devices is lattice matching the various semiconductor films so that detector and LED can be grown together with a reliable electrical interface. The limits set on absorbed and emitted wavelengths and efficiencies are sometimes deemed unacceptable, particularly if the emission cannot be brought into the visible range, and several strategies have been invented to overcome lattice mismatching. Most relevant to upconverter design is the wafer bonding technique, which works to unite two lattice-mismatched semiconductors which have been prepared separately and are fused as a near-final step.

Each surface is patterned with corrugations, and fusion demands that they be aligned for mating across the entire surface. Designing the photodetector and the LED independently is an important advancement, and the wafer bonding technique was first used by Ban et al. in 2004 to create a NIR upconversion device with ultimate (W/W) efficiency of 1.77 percent[13]. As the internal quantum upconverter efficiency was calculated as 76 percent at room temperature, it is evident that a most debilitating strike against efficiency comes from internal reflection at the semiconductor interface, where only ~2 percent of the photons can get out. A micro-lensed array of curved surfaces, with a greater solid escaping angle, was confirmed to release up to 40 percent more light (Figure 1.6.0); however, the device is still unsatisfactorily dim for many practical applications. Such micro-lens arrays furthermore introduce considerable complications into the fabrication process.

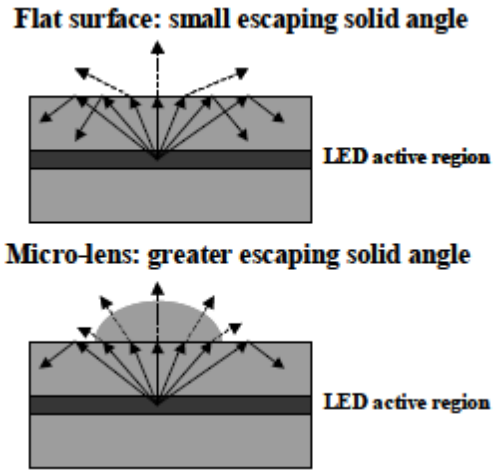

Figure 1.6.0: Solid escaping angles in flat and micro-lens surfaces[13]. The micro-lens array liberates more photons from the same LED, producing a greater external efficiency.

Wafer bonding evades the need to lattice-match photodetector and LED, but still demands the uniting of two substrates, entailing additional fabrication steps and the application of heat and pressure to the upconverter, which produces the non-uniformities present in FPAs. This thesis is dedicated to the more recent idea of a hybrid organic-inorganic device, with a photodetector founded on the InP and InGaAs systems and an organic LED deposited on top. The organic molecules used in modern OLEDs are not subject to the same lattice constraints as inorganic semiconductor crystals, as the organic layers are sufficiently pliable to conform to a surface without bulk strain. A single device with less complicated fabrication steps can then perform NIR upconversion.

1.7 Hybrid Inorganic-Organic Upconversion

Fully inorganic upconverters in the NIR range suffer from the restrictions of the lattice parameters or else the complications of wafer bonding, but at present inorganic photodetectors

(especially those founded of the InGaAs system) provide the best performance in the NIR range. Organic photodetector technology has not yet produced a competitive NIR candidate, but OLEDs are free of lattice parameter constraints and have recently achieved reasonable brightness. This thesis dwells on the advancement of hybrid inorganic-detector/organic LED devices.

1.7.1 OLED devices

The most basic OLED design consists of an emissive and a conductive layer placed between two electrodes[14]. Injected holes and electrons associate to form excitons in the emissive layer which may decay and release a photon of visible light by fluorescence; however, the up vs. down spin of these particles permits a total of four possible exciton combinations, three having net spin 1 (the triplet states) and one having net spin 0 (the singlet state). Ultimately, conservation of spin angular momentum only permits the decay and release of photons from excitons of the singlet state, resulting in a maximum internal quantum efficiency of only 25 percent in fluorescent OLEDs. Extracting photons from the remaining 75 percent of the excitons demands changing triplets to the singlet state by intersystem crossing; phosphorescent materials, bearing heavy metal atoms in complexes with organic molecules, have a strong spin-orbit interaction capable of changing triplets into singlets, and phosphorescent OLEDs can then approach 100 percent internal quantum efficiency.

OLEDs are vulnerable to a host of aging mechanisms that compromise their performance in the presence of oxygen and moisture, demanding an encapsulation strategy to protect the device under intermediary layers and introducing complications with light extraction through those layers. A refractive-index-matched layer is one potential solution; a consideration of

Fresnel's equations can conclude upon the ideal refractive index for an intermediary layer between the device and the air. Chemical changes of fluorescent and phosphorescent compounds in the bulk of the OLED layer can be instigated by electrical aging, and the roles of excitons and polarons in aging the interfaces between OLED layers is also an area of active research[15]. Strategies to quench excitons and prevent these aging mechanisms at the interface with surface passivation treatments can yield significant improvements in stability[16].

1.7.2 OLED on photodetector

In combination with the inorganic photodetector the OLED in the NIR upconverter will receive holes from the detector into its conductive layers. Atop the organic emissive layers the cathode of the OLED demands careful consideration: the need for solid electrical contact with a thick film is tempered by the need to let light escape the OLED for sufficient brightness (it is top-emitting, releasing light through the cathode). As previously discussed, internal reflection significantly reduces brightness of both OLEDs and inorganic LEDs.

In 2008 Ban et. al demonstrated such hybrid upconverters[17] with a design founded on a heterojunction phototransistor (HPT) detector bearing an OLED (Figure 1.7.0). A refractive index-matched layer was grown over the cathode to enhance light extraction. A further innovation in this work was the inclusion of a gold mirror layer between the detector and OLED, serving to enhance the performance of both elements simultaneously by reflecting both infrared light and visible light; reflected infrared light can pass through the detector a second time, and reflected visible light is redirected to the top of the upconverter in the direction of the viewer. Furthermore, hole injection from gold into the hole injection layers of the OLED is very efficient, bearing a low energy barrier. In contrast to the low W/W grade and temperature-

sensitivity of the first single-element upconverter fabricated in 1995, this device demonstrated an efficiency of about 155 percent (as the HPT consumed electrical power) at room temperature.

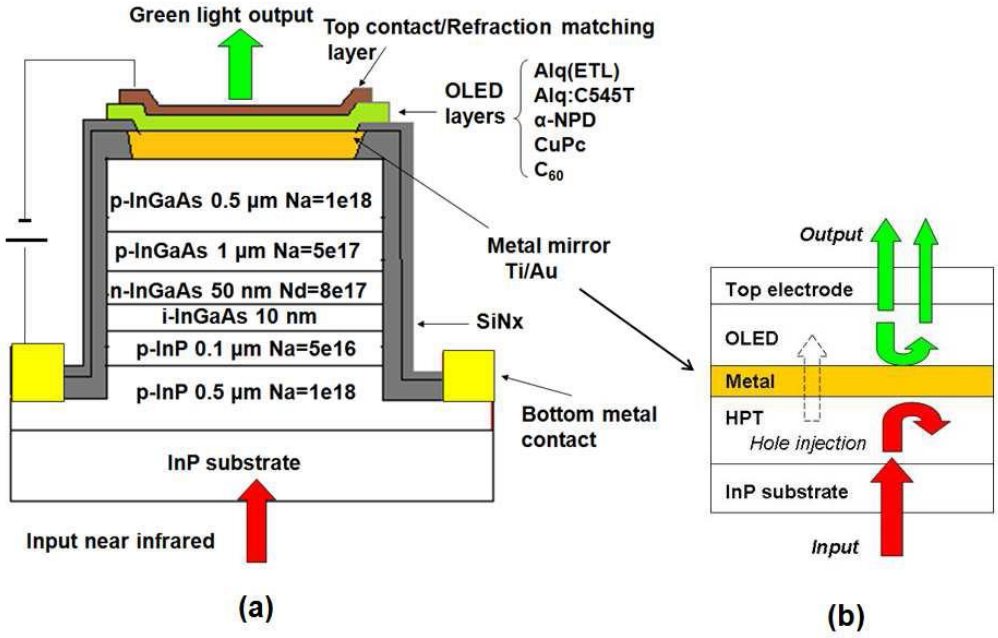

Figure 1.7.0: HPT photodetector matched with organic LED[17]. The HPT introduces an electrical gain to significantly improve the W/W efficiency of the upconverter. The full chemical names of organic compounds are provided in the List of Abbreviations. The presence of a gold mirror ensures good hole injection and simultaneous reflection of visible and infrared light.

However, the presence of a gold mirror is inconvenient in clean room facilities that deal heavily in silicon, as gold is a crippling contaminant of silicon, bearing an energy level close to the center of the silicon band gap. It is thus common practise for such facilities to minimize or outright ban the material from fabrication steps, and in such an environment the above design cannot be fabricated, as the gold-contaminated substrate is subjected to numerous additional fabrication steps which could conceivably hinder the work of fellow lab workers (gold would be tolerable only as a final step, with the substrate leaving the lab after mirror deposition instead of

receiving further processing). For this reason this thesis dwells on an upconverter without such a gold mirror; the leading alternative will be silver, which introduces a larger hole injection barrier and consequent complications and modifications to the OLED design. Aluminum mirrors and mirror-free designs will be also be discussed.

The upconverter designs previously considered included both pixelated and pixelless-arrays. Pixelated upconverter arrays will isolate carriers to prevent minimal lateral carrier diffusion, which would blur an image; in the absence of pixels this diffusion can produce detectable blurring, as depicted in Figure 1.7.1. NIR input shot through a stencil bearing a 132 micron shadow yields and upconverted image from a pixelless upconverter[18] with that feature blurred to 144 microns. Pixelated upconverters entail a more complicated fabrication process, however, and the topography of a mesa array presents a risk of topographic disconnection. Figure 1.7.2 underlines this difficulty with a similar upconverter device in the pixelated form[19], with compromised emission in the center of the array.

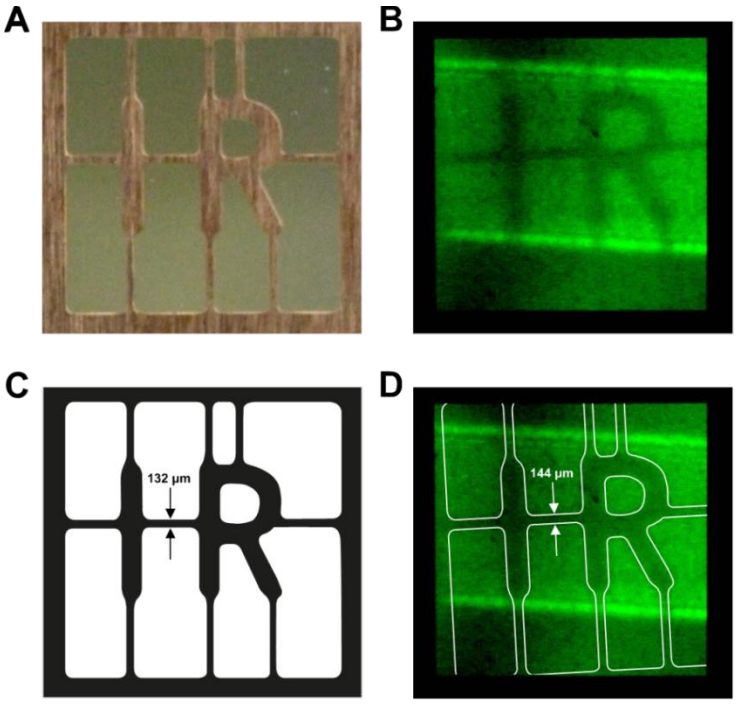

Figure 1.7.1: Pixelless upconverter results[18]. NIR input through a stencil pattern bearing a slender feature is upconverted into a visible image, demonstrating good full-cell emission from the OLED, but some blurring of the stencil features by ~10 percent by lateral carrier diffusion.

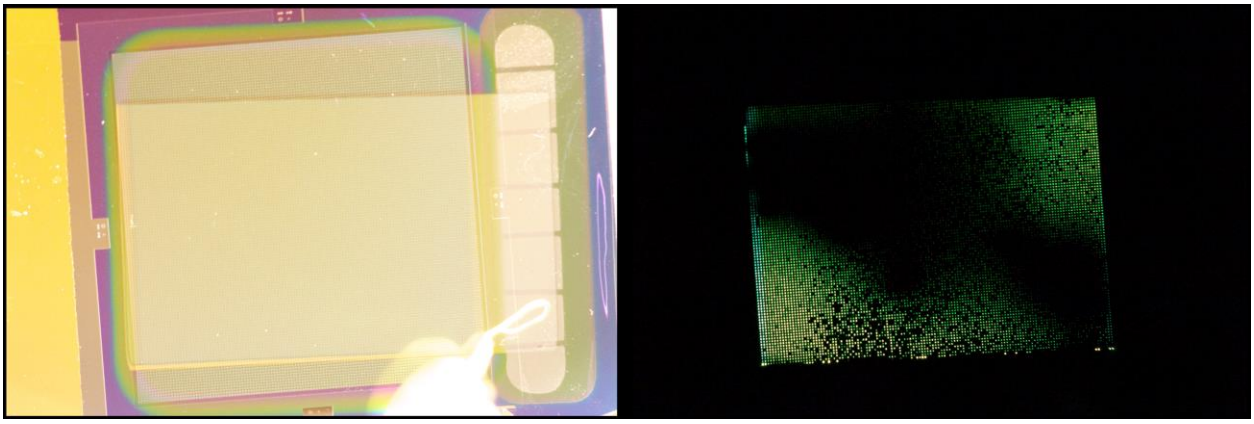

Figure 1.7.2: Pixelated upconverter array[19], demonstrating incomplete visible emission from large areas of the array in response to full exposure by NIR. One possibility, particularly relevant to this design, is topographic disconnection.

The following chapters will outline the fabrication, characterization and improvement of such Au-mirror-free hybrid NIR upconverters.

Chapter 2

2.0 Fabrication

All fabrication steps presented in this chapter are conducted in a strict clean room environment – besides limited dust a firm control of humidity and temperature is also generally essential for consistently successful fabrication. Moisture is particularly debilitating to the organic electronic materials used in OLEDs, which will age rapidly when tested (or even passively exposed) in ordinary air unless they are properly encapsulated.

2.1 Photodetectors

The photodetector elements that have proven workable in past upconversion devices include QWIPs, PN and PIN detectors, and heterojunction phototransistors (HPTs). Choice of detector element impacts performance considerably: the QWIP detectors used by Liu et al. are sensitive to a wide range of infrared radiation, but are crippled by a strong need of cryogenic conditions for efficient operation; the PN and PIN designs are the simplest to grow but generally possess lower responsivity (A/W) in comparison to other designs; the HPT detectors introduce an electrical gain to the detector circuit that can greatly amplify the number of carriers injected into the OLED, but they do so at the price of additional complexity in optimization, growth, and processing. PIN and HPT detectors were used in the experiments described in this thesis.

2.1.1 Wafer Growth

These photodetector wafers are grown by Molecular Beam Epitaxy (MBE), which entails heated source elements subliming into plumes in an ultra-high vacuum (~10^{-8} Pa). Such powerful

vacuums are generally achieved by cryopumps, which condense impurities on a chilled surface. These conditions permit precise and pure growth of semiconductor layers – the high vacuum conditions ensure that the plumes of source elements are effective beams that travel without collisions to the wafer[20]. Good quality layers of correct thickness demand constant monitoring of the surface during growth, typically accomplished by reflection high energy electron diffraction (RHEED), and rapid control of shutters over the source beams by a computer. The RHEED technique can distinguish layers down to one atom in thickness, and can precisely verify the ratio of different source atoms arriving at the wafer. Figure 2.1.0 outlines the main features of an MBE with a RHEED gun.

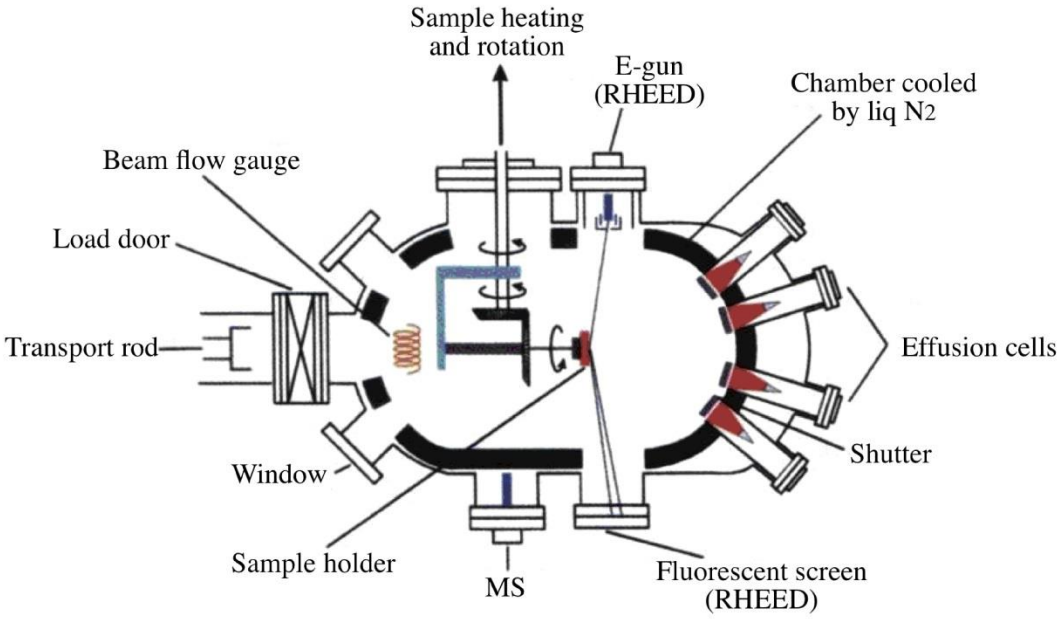

Figure 2.1.0: Schematic of standard Molecular Beam Epitaxy set up[21].

2.1.2 Wafer Cleaning

The essential cleaning process begins with wafer inspection through an optical microscope, looking for dust, scratches, residue, etc. If the wafer's surface is intact and useable it then

receives an acetone bath at 50 degrees Celsius, followed by a bath of heated isopropyl alcohol (IPA). Emersions generally last for 5 minutes each, and the wafer should be cycled between the baths at least twice, always finishing with IPA, which dries rapidly. (Specific times and recipes are variable between facilities[22]). Additional drying is accomplished by a nitrogen stream. Another inspection by microscope should be conducted to verify that previous imperfections have been cleared.

Further steps against any residual contamination can be taken by a Reactive Ion Etch (RIE) with oxygen plasma, using the Phantom II RIE system (Figure 2.1.1), which combusts unwanted organic material on the wafer. A short oxygen RIE burst ensures extra cleanliness, but will produce a thin layer of oxide at the wafer surface. This oxide interrupts the photodetector with an insulating layer and needs to be removed before subsequent steps are taken. Brief emersion in dilute hydrochloric acid can be used to strip off this oxide layer. This complication from RIE treatment is necessarily only acceptable if the top layer of the photodetector is sufficiently thick (>10 nm), or else the cleaning process may thin, hole, or outright remove that peak layer. Chlorine ions that are not properly cleared can also negatively impact the eventual OLED performance[23] by acing as fluorescence quenchers.

Figure 2.1.1: Phantom II RIE system[24]. A hybrid physical-chemical etching system, RIE is simultaneously capable of some material selectivity and an anisotropic etch progression.

2.1.3 Photolithography

Proper cleaning is essential for photolithography with consistent and sharp features. It is generally critical that an adhesive layer is first applied to the cleaned substrate. A typical choice as an adhesive layer is hexamethyldisiloxane (HMDS), which is spun on the wafer and then dried on a hotplate to produce a very thin (~1 nm) layer that adheres well to both the substrate and the typical photoresist recipes.

The typical photoresist, used here, is the product of the AZ Electronic Materials company: these resists bear diazoquinone, which reacts to ultraviolet exposure by producing nitrogen gas and carbenes[25]. Spinning at high speeds ensures more uniform layers, but this becomes more complicated in subsequent photolithographic steps in which the wafer is no longer flat due to the mesa features of the detector. Photoresist spinning over mesas can lead to ‘snowdrift’ phenomena, with resist piling up on one side of a raised feature and potentially

leaving other areas bald. Consequently, the fastest spin recipes should generally be used on the initial flat wafer. After spinning it is necessary to pre-bake the resist on a hotplate to minimizing any sticking of the sample to the mask, which would complicate alignment before exposure.

Exposure by mercury lamp (selecting the 365 nm wavelength in this case) is done following precise alignment with the Karl Suss MA6 Mask Aligner (Figure 2.1.2), which can be a complicated task depending on details of the pattern and the size of the wafer. Any adhesion by the photoresist to the mask generally forbids or cripples alignment – a sample that sticks generally must be receive more pre-baking exposure.

Figure 2.1.2: Karl Suss MA6 Mask Aligner[24]. A sample is aligned with a glass plate bearing the mask pattern (written in Cr here), and exposed with a UV lamp to selectively expose the photoresist with the mask pattern.

Development may proceed rapidly and should be observed by eye for the largest features which may be visible, and may be finished within 30 seconds. A typical developer, used in the fabrication of devices discussed here, is the AZ 300 MIF developer, which consists primarily of

tetramethylammonium hydroxide (TMAH). Following development the features should be inspected by microscope to ensure that edges are straight, corners are sharp, and that the alignment marks are particularly well-formed for subsequent photolithographic steps. After acceptable features are confirmed post-exposure baking of the substrate is recommended to eliminate any residual solvent in the photoresist layer.

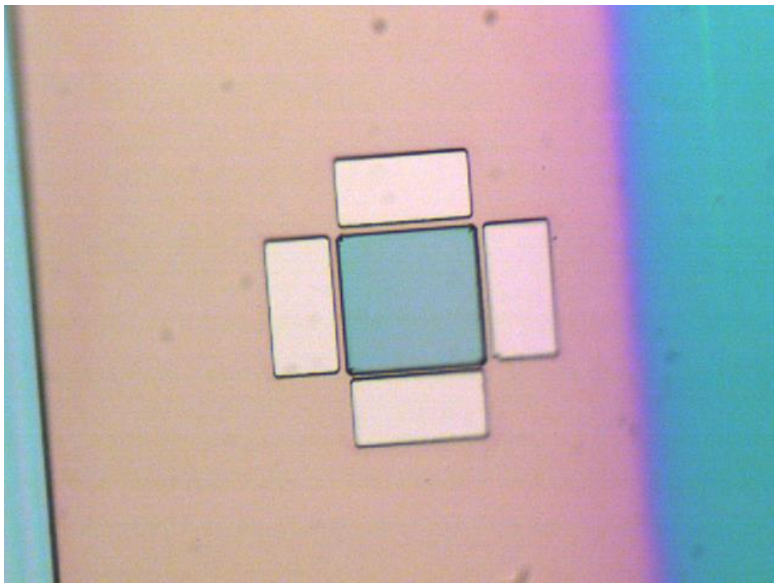

Figure 2.1.3: Mask alignment feature verification between two layers of the photolithography pattern.

2.1.4 Mesa Etching

Electrically-isolated mesas need to be etched into the photodetector surface in most upconverter designs. The etch proceeds through the photodetector layers to the substrate, allowing a bottom contact to be made later. This etch can be complicated by non-uniformities both across the area of the wafer and down the cross-section of wafer layers. To achieve a precise depth the chemical etching process must be interrupted and measured frequently.

Sulphuric acid, hydrogen peroxide and water combine to produce the 'piranha' etch solution. This recipe is both corrosive and explosive, making safety precautions paramount while creating, using and disposing of this solution[26]. One critical detail is that piranha etch must not be stored, as in a sealed container fumes can accumulate. After the etching process is completed the piranha solution must be destroyed by neutralizing, typically by chips of potassium hydroxide. Precise control of etch depth generally favors a dilute recipe: in this work a recipe of 1:8:320 parts H_2SO_4:H_2O_2:H_2O was used to achieve fluctuating etch rates between 220 and 460 nm per minute through InGaAs layers (bearing a range of doping concentrations). Figure 2.1.4 shows the result of a controlled etch with good features seen through an optical microscope.

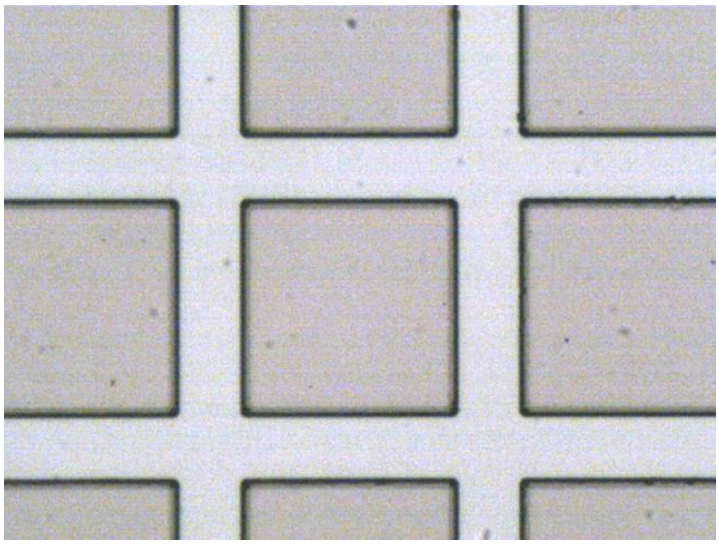

Figure 2.1.4: Square mesas etched into the wafer surface by the piranha solution.

2.1.5 Insulation and Window Etching

Deposition of an electrical insulation layer is critical to prevent shorting of the eventual photodetector and upconverter. This layer will have windows opened up to permit top and bottom contacts to the mesas. Silicon nitride and silicon oxide can each serve as adequate passivation layers, but the vacuum level of the deposition chamber may introduce significant

faults in the crystal structure. Such imperfections may include voids in the passivation layer, and significant surface roughness. The former problem can be addressed by increasing the thickness of the insulation layer to ensure that there are no electrical shorts; the latter problem complicates the subsequent photolithography, and can be addressed by RIE etching.

In previous trials using SiN layer thickness ranging from ~400 nm to as low as ~200 nm were successfully used to electrically isolate mesas. This SiN film was deposited by the PlasmaTherm 790 Series Plasma Enhanced Chemical Vapor Deposition (PECVD) system, which produces high-quality layers. However, the PlasmaTherm system demands a significant amount of time to achieve a low vacuum pressure, which is a particular inconvenience in a shared clean room environment. SiO_2 deposition using the Intlvac E-beam Evaporator system can produce insulation layers more rapidly, but the use of a lower-quality vacuum results in a layer bearing more voids and impurities, and greater surface roughness. E-beam deposition of SiO_2 was used to insulate the photodetectors under discussion here by accommodating for these imperfections.

To test the usability of this system layers of ~700 nm were deposited by the Intlvac E-beam Evaporator (Figure 2.1.5), and profiling with the Dektak 8 Stylus Profilometer confirmed that this SiO_2 layer was indeed rough with islands raised up to ~50 nm above the sample surface. This surface roughness would jeopardize the uniformity of the photoresist layer that would follow in the windowing opening process, and so the film's thickness is reduced to ~600 nm by etching the substrate with CF_4 plasma in the RIE chamber. Profiling subsequently confirms that the 100 nm etched-back layer has significantly reduced island height, with an improved roughness within ± 10 nm. Subsequent work explored variations on the thickness of the oxide layer. While thicker layers resist shorting, an issue that appears in the photodetector and upconverter results, a thinner layer produces a smaller topographic step for OLED and cathode

layers to traverse, and topographic-based disconnection also bears some likely responsibility for low currents observed in some devices, as well as incomplete cell performance observed in the upconverters that preferentially favors the edges of cells.

Figure 2.1.5: Intlvac Thermal/E-beam Evaporator (left and right chambers, respectively), with a nitrogen glove box above[24]. After samples are loaded the chambers are pumped to a low vacuum, and the same is exposed to a plume of ejected material instigated by Joule heating or e-beam exposure, respectively.

Following the etch-back process the smoothed SiO_2 layer is subjected to a second photolithographic process to produce open windows of photoresist over the mesa tops after development. Figure 2.1.6 illustrates a successful photolithographic process ready for window-opening.

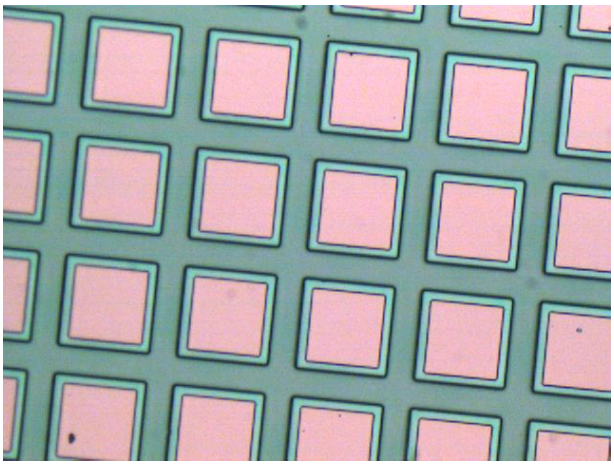

Figure 2.1.6: Mesas covered in photoresist after development, showing windows on the mesa tops which can now be etched open.

Once this is confirmed window opening can proceed by either dry or wet etching of the SiO_2 film to expose the top layer of the photodetector (Figure 2.1.7). A dry etching process produces vertical sidewalls, but the imperfections in the wet etch process are countered by greater selectivity: a dry etch done carelessly will eliminate the insulation layer and continue into the detector's top layer, which may be damaged or, if negligence is extreme, removed. Dry etches are essential if the device features in the mask are particularly small and have little tolerance for the creep of a wet etch. However, if the features are large enough to tolerate such creep the wet etch method will be useful in that it generates a slope rather than a discrete step of insulation material on the border of the opened window, which may be to the benefit of the subsequent OLED layers by reducing the risk of topographic disconnection.

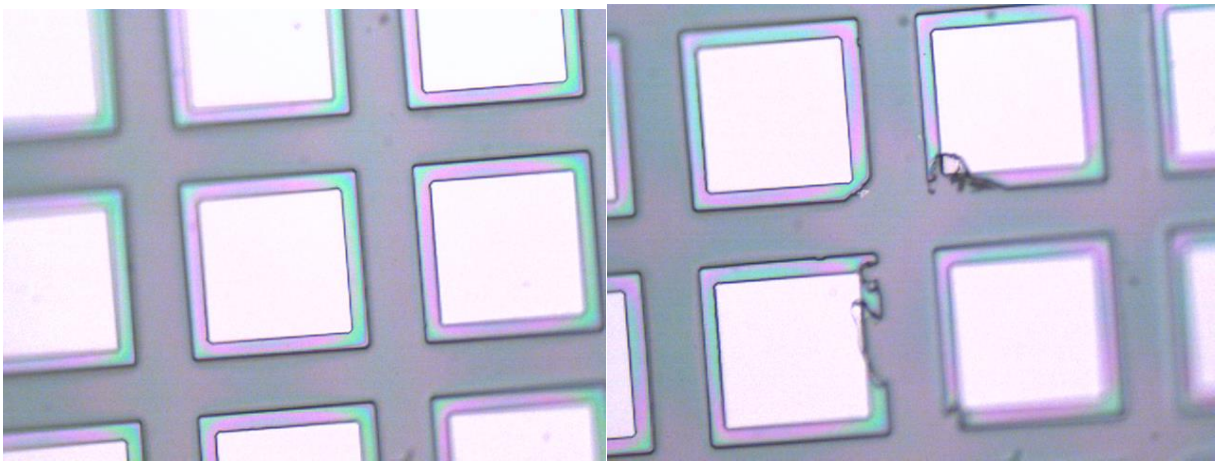

Figure 2.1.7: Opened windows after etching, presenting the top photodetector layer, insulated with silicon oxide. At left: good opening with minimal damage to the photoresist border during etching. At right: imperfections in the border resulting in malformed mesas.

In the devices under consideration here a dry etch process with CF_4 plasma in the RIE chamber (the very same recipe used to perform the etch-back and smooth the insulation layer for photolithography) was explored at first, and compared to a wet chemical etch process using buffered hydrogen fluoride (BHF) to selectively eliminate SiO_2 with minimal risk to the top layer of the photodetector. The device patterns in use were not required to be particularly small and so could tolerate the creep of a chemical etch process. In either process the etch must proceed to completion, perhaps to the point of sacrificing the integrity of the top photodetector layer, as even a minimal layer of ~1 nm remnant oxide would be sufficient to interrupt the electrical contact between the detector and the OLED, and this layer would not be detectable by a profilometer beforehand.

After etching has been completed the photoresist is to be cleaned thoroughly, and the insulated mesas and windows are to be examined for significant cracks and other defects before proceeding (Figure 2.1.8).

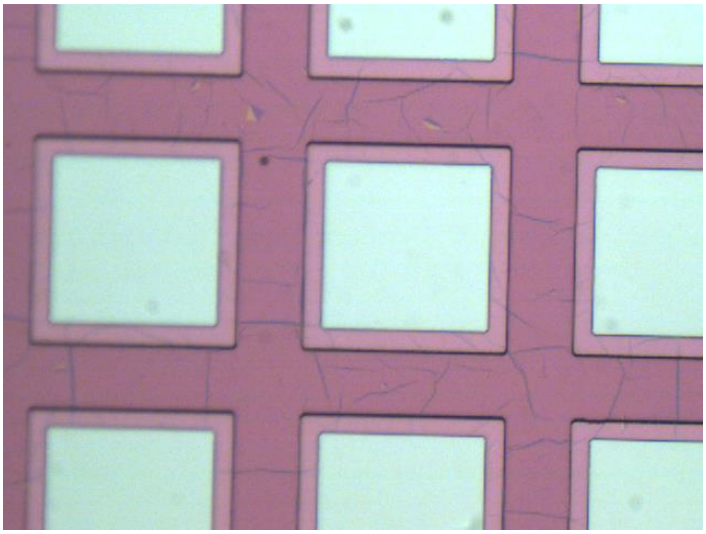

Figure 2.1.8: Cleaned mesas with windows through the oxide layer. Imperfections in the oxide layer appear as cracks, but the layer's high thickness ensures electrical insulation. Thinner layers, with less risk of topographic disconnection, are more vulnerable to shorting due to such faults.

2.1.6 OLED surface preparation

After windows have been opened and the photoresist removed the photodetector needs to be prepared for the application of the OLED. In both mirrored and mirror-less designs the top layer of the photodetector need to be passivated to ensure that the device's photocurrent when exposed to infrared light will be significant compared against the dark current; without passivation significant carrier recombination can occur at the mesa surface. HCl and ammonium sulfide are typical choice solutions for passivating layers of InP and InGaAs[27, 28].

In designs seeking high efficiency a reflective mirror is deposited between photodetector and OLED to enhance the performance of both: the mirror reflects infrared light back for a second pass through the detector, similar to the *tapetum lucidum* (or 'eyeshine') found in the eyes of cats and other nocturnal animals; the mirror also reflects the visible light of the OLED to increase the number of photons which are released in the direction of the viewer.

A mirror of gold shows good reflectivity in both the infrared and visible range (Figure 2.1.9), serving both intended purposes. Gold is also a useful anode material for OLEDs due to is high work function, which presents a low injection barrier for holes entering the OLED. However, gold is a notoriously bad material to use in a standard fabrication facility because it is a crippling contaminant of silicon, bearing an energy level near the center of silicon's band gap. Consequently it is a standard practise for silicon-bearing fabrication facilities to minimize or outright forbid the deposition of gold and post-processing steps that could contaminate other wafers with gold. For this reason the gold mirror used in previous upconverter designs[17] was abandoned in favor of a silver-based mirror, producing a novel design.

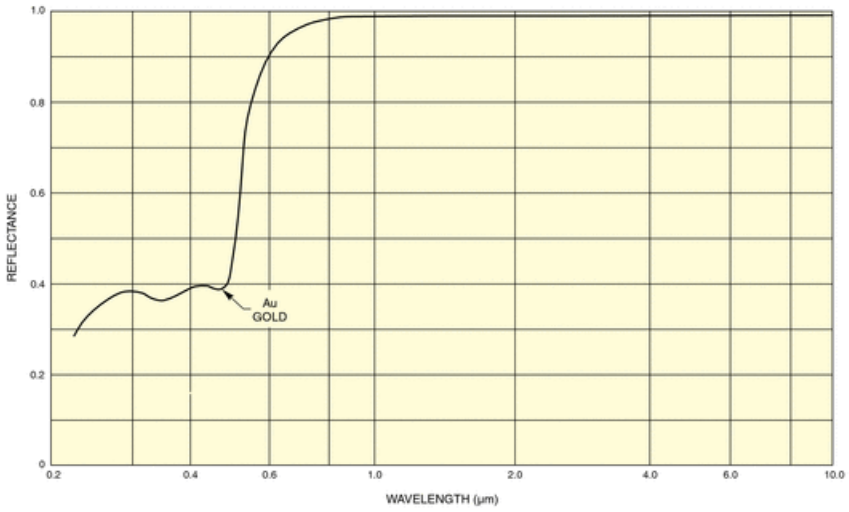

Figure 2.1.9: Reflectivity of gold at and above visible wavelengths[29]. Au is highly reflective in the infrared and will reflect about 80 percent of the OLED's 525 nm green light.

Silver, despite its good reflectivity properties, is an inferior choice as an anode material for OLEDs, as it bears a small work function and a significant hole injection barrier. Modifying the silver layer prior to deposition of the organic layers has been accomplished by previous

OLED and organic solar cell groups[30, 31], which induce a surface-dipole effect with thin layers of CF_4 or Ag oxide to modify the work function[32]. However, these strategies are time-sensitive, like conventional surface passivation of InGaAs and InP, with the surface-dipole layer being sufficiently volatile to have holes or to have outright dissipated by the time a wafer brought to a low vacuum for OLED deposition. Consequently, surface modification of the silver in the vacuum, using molybdenum oxide[33], followed immediately by organic layer deposition, was employed in fabricating the Ag-anode OLEDs and mirrored devices of interest to this thesis. Large area deposition of metal introduces a shorting issue which will be discussed in the next chapter.

2.2 OLEDs

OLED performance is highly sensitive to many parameters: the vacuum quality of the deposition chamber, the purity of the materials, the rate of deposition, and the atmosphere of storage and testing. It is consequently necessary to establish good OLED recipes for a particular deposition system rather than trust a generic recipe to perform.

Figure 2.2.0 below present the structure of a green (~525 nm emission) OLED bearing a CuPc hole injection layer (HIL), NPB hole transport layer (HTL), and an Alq_3 electroluminescent layer (see List of Abbreviations for complete chemical names). These particular materials are well-established in the production of bright and stable fluorescent OLEDs. As discussed in section 2.1, the choice of a silver anode (in place of the more optimal gold) demands modification of this more standard OLED design to ensure efficient hole injection into the HTL. Maintaining NPB and Alq_3 ensures the ~525 nm emission, but modifications to the cathode and anode of the OLED are necessary for this particular device.

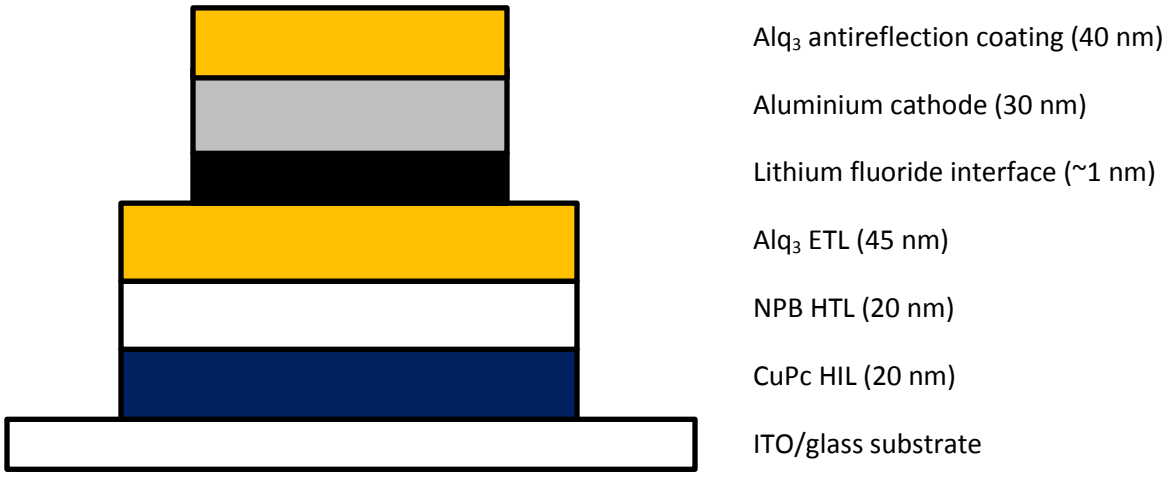

Figure 2.2.0: Trial OLED structure.

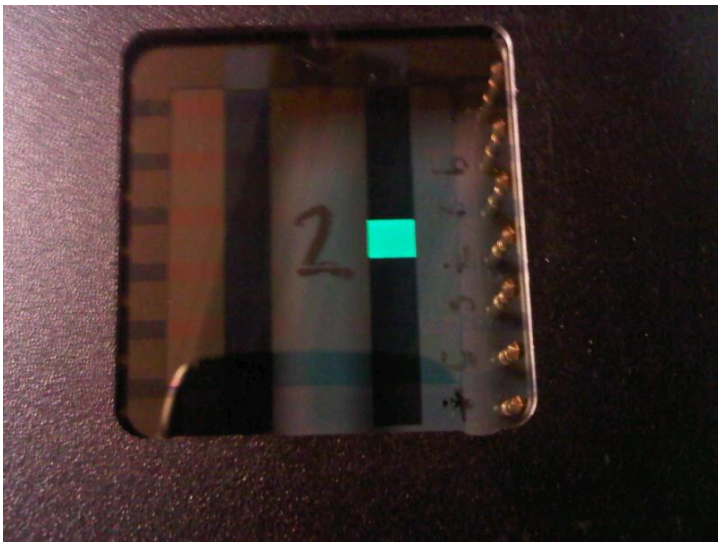

Figure 2.2.1: An OLED cell of the discussed structure emitting at ~525 nm.

In particular, hole injection into NPB from Ag is normally very inefficient, with an energy barrier approaching 0.8 eV (in contrast to the barrier of injection from Au, which is <0.1 eV)[17]. Modifying the Ag surface can change the work function to lower this barrier and improve injection, and in the experiments of this thesis Ag surface modification was accomplished by applying a thin layer of MoO_3. As with other strategies to improve Ag anode

hole injection the MoO_3 bears a surface dipole property to adjust the work function of Ag at the surface, improving hole injection efficiency by reducing the energy barrier. Such methods are generally explored by researchers in the effort to make OLEDs with transparent anodes[31], as the high conductivity of Ag permits a thinner layer to serve as an adequate electrical contact, reducing absorbed light.

MoO_3 was selected of the available surface treatments due to the ability to swiftly continue the deposition of organic material after the MoO_3 deposition in the chamber with the available equipment. Hole injection from Ag anodes has also been improved by RIE treatments with O_2 and CF_4 (similar to recipes also used to passivate ITO) to passivate Ag[31, 32]. However, these are all treatments that would be conducted outside the deposition chamber, followed by a delay as the sample is mounted and brought to vacuum in the chamber to begin the deposition. This delay is problematic for a volatile surface treatment which may be degraded by exposure to oxygen and moisture, such that large areas of the device would lose their passivation by the time the organic material is actually deposited. MoO_3 can be deposited on the Ag within the chamber with the available equipment, followed immediately by OLED materials while maintaining a high vacuum, nixing any possibility of passivation corruption by volatility.

Efficient electron injection from the cathode into Alq_3 is conventionally accomplished with an Al layer separated from the Alq_3 by a thin (~1 nm) layer of lithium fluoride (LiF). As in the case of Ag anode modification by MoO_3, LiF modifies the Al work function directly in contact with the OLED to significantly improve carrier injection efficiency[34]. While Al is inferior to Ag in terms of electrical conductivity, demanding a thicker layer and reduced transparency, the good electron injection efficiency of the Alq_3/LiF/Al combination justifies its use in the experiments discussed.

Thinner layers of organic material are more vulnerable to non-uniformities, with very thin layers being prone to pinch points and even gaps which may ruin the device by serving as electrical shorts. Thicker layers, however, introduce greater resistance to the OLED, so it is necessary to optimize the dimensions of multiple layers systematically to produce an OLED that is bright, has good uniformity across a device and between multiple devices. Figure 2.2.2 outlines the consequences of varying the NPB layer thickness in OLED devices: while the 10 nm thickness produces a brighter emission, this emission is less consistent across multiple devices and less stable over prolonged testing in comparison to OLEDs with thicker layers.

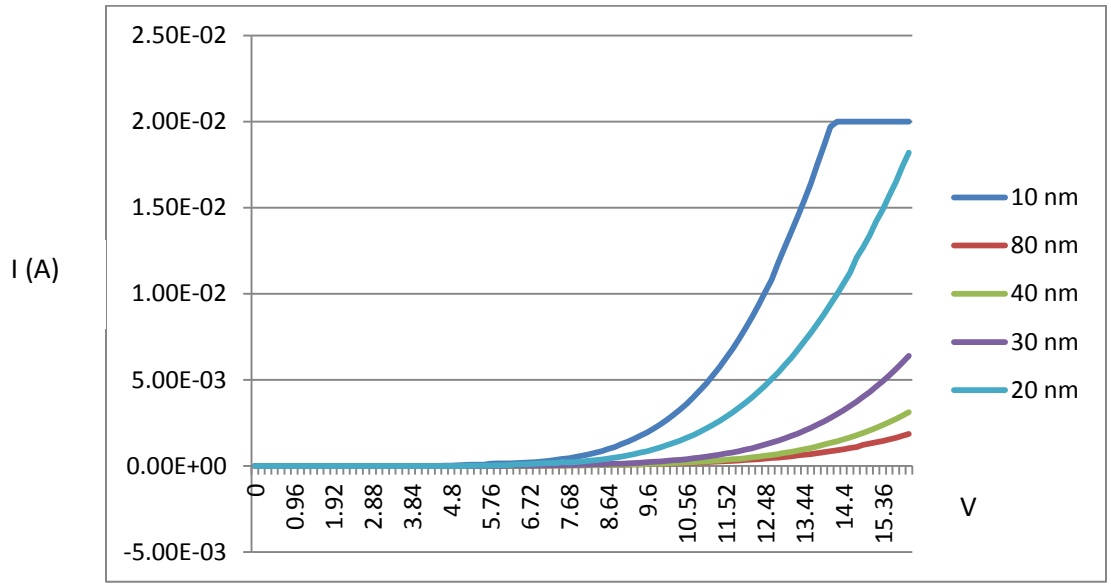

Figure 2.2.2: OLED designs with varied hole transport layer (HTL) thicknesses, demonstrating the consequences of increasing resistance. The thinner layers present uniformity problems, however. The saturation at 20 mA is an artifact of the testing apparatus.

Deposition is done in a high vacuum chamber through a shutter mask, which ensures that organic and electrode materials are only applied to desired areas of the device. The mask bears multiple patterns which can be extended or retracted as required to bring a pattern into alignment

with the sample, allowing different layers to deposit through multiple mask patterns on a single substrate without breaking vacuum. Moisture and oxygen contribute to the aging of the organic layers in OLEDs, so ensuring high vacuum throughout the deposition process is critical.

After deposition the samples should be tested immediately, before they can be aged by any incidental exposure to air or oxygen (even the nitrogen environment available in the clean room will possess some relevant impurities). OLEDs are also susceptible to electrical aging, however, so it is important to establish and respect the range of voltages that can be applied to a particular OLED design without significantly degrading its performance. In general, thinner layers of organic material are more susceptible to electrical aging processes, which occur even when the sample is tested in a nitrogen flow.

Chapter 3

3.0 Characterization of Photodetectors and OLEDs

Photodetector and OLED devices must naturally be tested separately to ensure good performance before they are combined into the upconverter. Such testing is most useful when the separated devices are made as representative as possible of the detector and OLED that will appear in the upconverter, which may entail careful fabrication design. In particular, it was found that many OLED designs that work well on a glass substrate bearing an Ag anode (representative of the Ag mirror to appear in the final mirrored upconverter) fail to emit well, or at all, in a reasonable voltage range when deposited onto the photodetector. Details of surface roughness, particularly the steps of the window border and the mesa, can interfere with an OLED design of any quality, and the OLED's presence introduces extra resistance to the electrical circuit, impacting detection efficiency; furthermore, probing such a device properly, without piercing layers of insulation or inviting conduction through alternative and non-emissive paths, is an additional concern.

3.1 Photodetectors

3.1.1 Evaluation

The responsivity (A/W) of a photodetector is its primary metric of evaluation of interest in this thesis. To account for relevance of signal-to-noise ratio the current used to calculate the ultimate responsivity will be the photocurrent, subtracted the detector's dark current from the absolute current.

Collecting an accurate measurement of the watts of NIR light that the device receives is also crucial in developing this metric, and the laser source used in the characterization must be

verified by a power meter bearing its own calibrated photodetector (for improved certainty, two such detectors are compared with each other independently to verify a power reading). The power actually delivered to the laser surface is not a straightforward emission from the laser, however, as the beam's collimation is not perfect: the separation and any intervening optics between the laser and the photodetector will adjust the power ultimately delivered, which must be routinely checked with each round of measurement to account for any fluctuations in performance and geometry. Statistical noise is a reality in these measurements, which are taken multiple times to the end of producing a consistent average.

One severe complication in testing the photodetector is the angle of exposure by the laser: any exposure from above will be compromised heavily by a mirror (which is intended to reflect the IR light). More ideal exposure, from the bottom, may not be permitted in some characterization setups, as the photodetector must sit on a stage to be properly probed. Even in the case of ideal exposure from directly below, the substrate of the photodetector can be expected to absorb some IR light, and certain materials (p-doped InP) may actually absorb so much IR as to make bottom IR exposure minimally effective. The seemingly arbitrary NIR powers seen in the following plots are powers measured from shooting the laser through each particular substrate; for example, 50 mW/cm^2 initial laser power is reduced to 1.36 mW/cm^2 due to substrate adsorption (and any failures in collimating the beam).

Useful probing demands precision in all three dimensions with fine-tipped pieces, ideally verified with an optical microscope. The application of pressure to the detector by the probes is a very precarious maneuver – some pressure is required to ensure a good electrical connection, as otherwise the probes may bounce on the surface due to slight vibrations (as they are exposed to air), but too much pressure with a sharp tip will allow the probe to pierce layers of the device,

including the insulation layer. Furthermore, inappropriately high pressure will damage the probes, bending or breaking them and making subsequent measurements less reliable.

Figure 3.1.0 demonstrates a photodetector response to NIR exposure, with a photocurrent in the mA range.

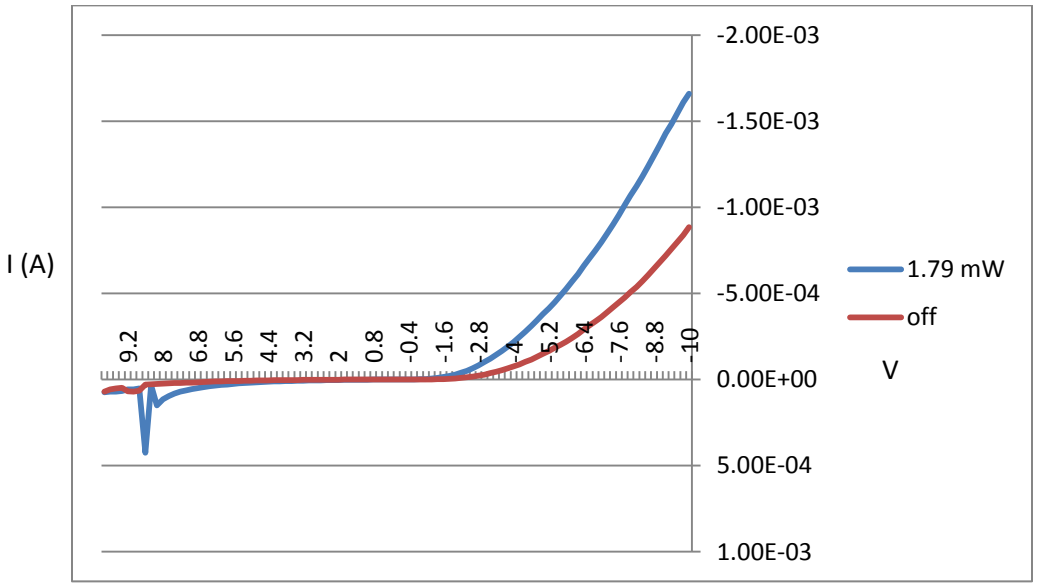

Figure 3.1.0: mA photocurrent response of an HPT photodetector to NIR light.

When considering more scans taken over greater time, however, this photocurrent response is shown to loose good consistency with increasing NIR exposure. Responsivities collected over extended probing were measured to expected values in isolation, despite inconsistencies in considering multiple values collected over an extended period of probing. Figure 3.1.1 shows a responsivity saturating at approximately 0.35 A/W on a detector thought to have an ideal responsivity of 0.5 A/W, indicating that proper probing does allow verification of detector performance.

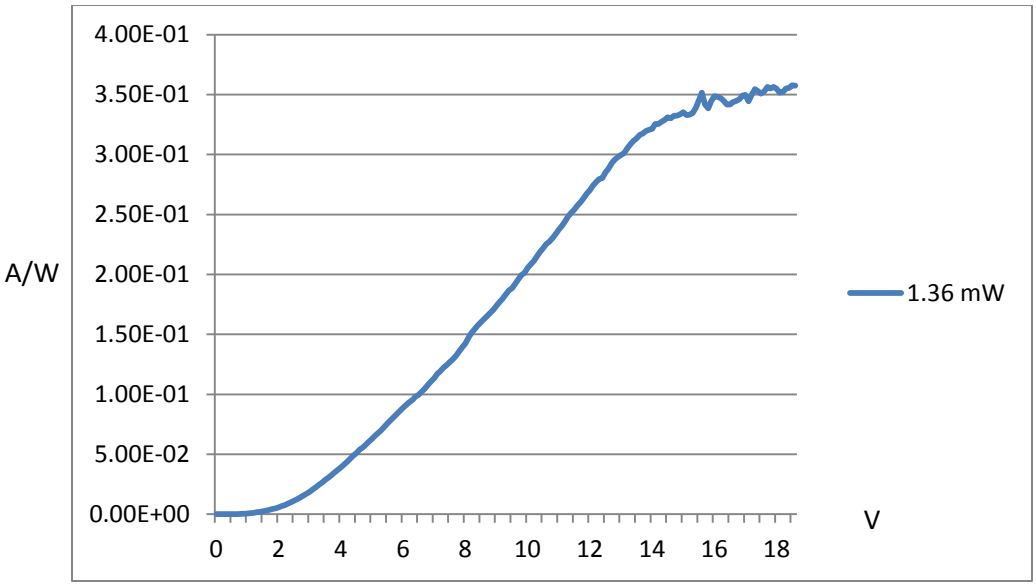

Figure 3.1.1: Responsivity of an HPT photodetector to NIR light, achieving ~70 percent of the ideal value.

3.1.2 Photodetector faults

The ideal behavior of a photodetector differs significantly from several measurements taken. Despite the measurement of a mA current and the realization of a reasonable detector responsivity the results are transient between scans, and in some cases transient within a single scan, likely demonstrating faults in the characterization set up. Exposed to air, vibrations and movement of the probes, changing xy position, are conceivable, particularly when the setup is not isolated in a box but exposed in a lab space bearing other equipment, ventilation, and other potential sources of noise. In addition to xy variability the z position of the probe can be adjusted to produce bouncing on the surface, changing the total probe area in contact with the same and compromising the ability to compare multiple scans or even values collected within a single scan. When the probe is set down firmly to negate any chance of bouncing and transient contact the probe is put under tension, which may relax to change the contact.

A more debilitating source of non-ideality would come from faults in the fabrication of the photodetectors; etches not concluded at the proper depth, incomplete or flawed insulation layers, damaged peak layers, incomplete cleaning, etc. The integrity of the silicon oxide insulation layer, particularly at a reduced thickness in trials made to account for topographic disconnection in the eventual upconverters, is questionable in particular due to shorting issues observed whenever a mirror was attempted on these photodetector cells. Metal intruding into pores or cracks in the insulation, circumventing the photodetector mesa to produce shorted currents, is suspected to have occurred in all Ag- and Al-mirrored devices, despite the insulating property of the latter's oxide. Damage to the top layer of the photodetector was thought to be a more secondary explanation, as this mirror-shorting was observed in samples both dry and wet-etched, with the latter's selective nature being far less likely to intrude into the InGaAs layer and cause significant flaws.

Wet-etched samples are furthermore expected to possess slopes in place of steps at the edges of device features, making OLED conformity issues and topographic disconnection less likely. In such cases it therefore expected that the upconverter can tolerate thicker layers of insulation to avoid such shorting issues. However, as a single fault across the entire cell can introduce a short, it was found that even insulation in excess of 500 nm demonstrating mirror-shorting. This may indicate a quality of oxide too poor to resist metal intrusion, and recommend the choice of a superior material and/or deposition system with a higher-quality vacuum. The CF_4 RIE etch-back process used upon the oxide to make it planar and suitable for photoresist spinning and lithographic processing may be introducing the suspected faults.

3.2 OLEDs

3.2.1 OLED characterization on glass

The rapid aging of organic materials in moisture and air demands that OLED testing be done in a controlled environment, ideally of intimate flowing nitrogen. OLED testing is consequently conducting in a test box with a nozzle permitting the attachment of a tube carrying flowing nitrogen. The test box bears a mechanical set up of probes designed for the particular patterns of the glass test substrates which are used to evaluate OLED designs in isolation, confirming their functionality.

Brightness, stability, and consistency across devices are critical parameters in this characterization. The turn-on voltage, and the efficiency of the OLED (Cd/A) are also worth calculating and considering, as the ultimate performance of the eventual upconverter will be graded by considering the W/W ratio of input and output light, which is the product of the detector's responsivity (A/W) and the OLED's external luminescence (W/A).

The OLED designs are limited by the sophistication of the available deposition equipment: some setups bear multiple chambers and can produce nearly-arbitrary structures of many layers, thicknesses, and precise doping levels of phosphorescent compounds as multiple materials are deposited simultaneously. The fluorescent OLEDs grown in the work of this thesis were grown in a single chamber permitting only one material deposition at a controllable rate at once: multiple depositions with such a system invite inhomogeneity in relative amounts as rates fluctuate, and the performance of OLEDs with doped layers has a critical reliance of precise doping levels (accurate to within ~1 percent). Thus, most OLEDs grown in this work have undoped layers of one organic fluorescent material.

Figure 3.2.0 displays the averaged luminescence of a well-made OLED grown on a test substrate of glass bearing ITO (which received a 50 nm layer of Ag to simulate the mirror of the complete upconverter). Ten devices and made and probed on this representative substrate demonstrated luminescence from 3 000 to 10 000 Cd/m^2, which remained consistent over extended testing. In keeping with the reservations expressed earlier in this chapter, however, an identical design deposited on an upconverter does not produce a significant emission due to complications with the mirror/OLED and detector/mirror interfaces, as well as the potential for topographic disconnection not present on a flat glass substrate: such tests are not perfectly representative.

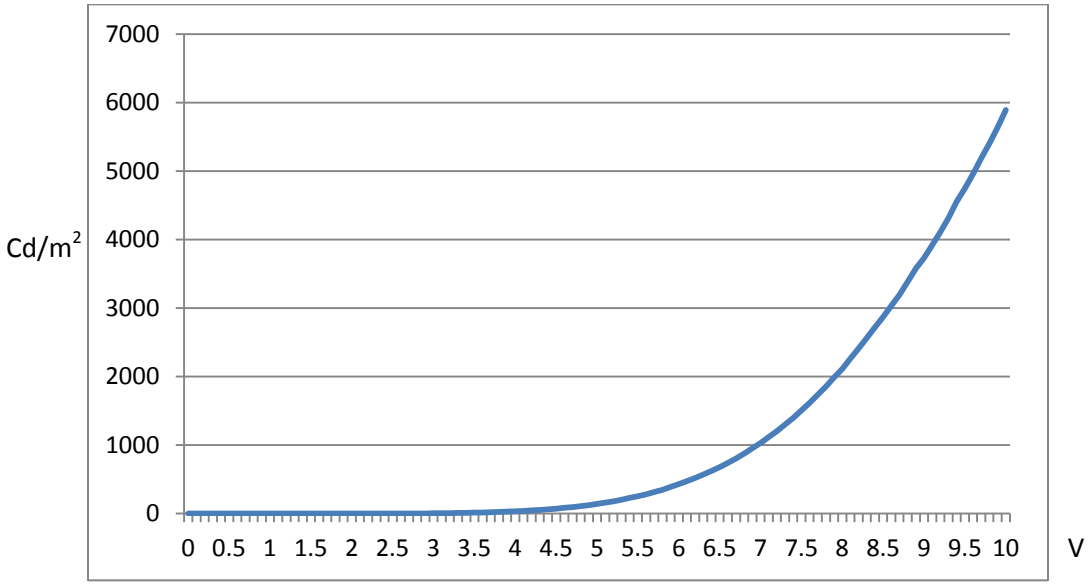

Figure 3.2.0: OLED devices grown on simulated Ag mirror, demonstrating good intensity and stability.

3.2.2 OLED faults

Numerous aging mechanisms plague OLEDs, limited their lifespans, emission spectrum, luminosity and stability.

In the fluorescent OLED devices discussed in this thesis the electroluminescence layer consisted of Alq_3, and so its particular aging mechanisms are most relevant. In the presence of water Alq_3 can degrade into chemical products that act as luminescence quenchers by thermal hydrolysis[35, 36], a reaction that becomes increasingly relevant at high heat and oxygen pressure. Such thermal hydrolysis of Alq_3 is most relevant in the OLEDs deposited on photodetectors discussed in the following chapter.

Molecular oxygen can also serve as a fluorescence quencher[37], such that even exposure to perfectly arid air will degrade the OLED. This demands that experiments be taken with minimal delay after deposition and in quick succession; otherwise the full OLED's performance will not be captured, and comparisons between data points will become meaningless.

A final experiment featured in section 4.4 presents the results of an upconverter bearing a phosphorescent OLED, which is subject to some different potential faults. OLEDs of this design offer powerful advantages over fluorescent OLEDs by allowing intersystem crossing to liberate triplet excitons into singlets, exceeding an external quantum efficiency of 25 percent; the most vexing limitation of phosphorescent OLEDs, that the blue ones are limited in lifespan, is not relevant to the upconverters under consideration here, which emit a single wavelength to display binary presence/absence of infrared light. (Future generations of upconverters may consider OLEDs of different colours to independently upconvert and display distinct wavelengths of infrared in a single display).

Quenching phenomena debilitating fluorescent OLEDs is relevant to phosphorescent OLEDs as well, but loss of triplets is now relevant: triplet-polaron quenching[38] degrades from ideal performance in these devices. Chemical changes in the bulk of the emissive layer can yield the polarons able to interact with triplets and waste their energy as phonons.

Chapter 4

4.0 Upconverters

4.1 Direct combination

One significant issue with developing the upconverter is the nonlinear appearance of higher resistance associated with combining the detector and OLED elements. Comparing Figure 3.1.0 with Figure 4.1.0 below, it is evident that the resistance in effect on this device by the application of an OLED has been increased by a factor of ~10^5 from an initial (bare photodetector) value of ~15 kilo-ohms to 2 giga-ohms despite the fact that the OLED in isolation only possessed 8 kilo-ohms of resistance to be added in series. More than 99 percent of the high resistance shown here is a consequence of interface and topographic issues complicating the straightforward linear combination of detector and OLED. The low currents in such a device produce no significant emission from an OLED that works well in isolation.

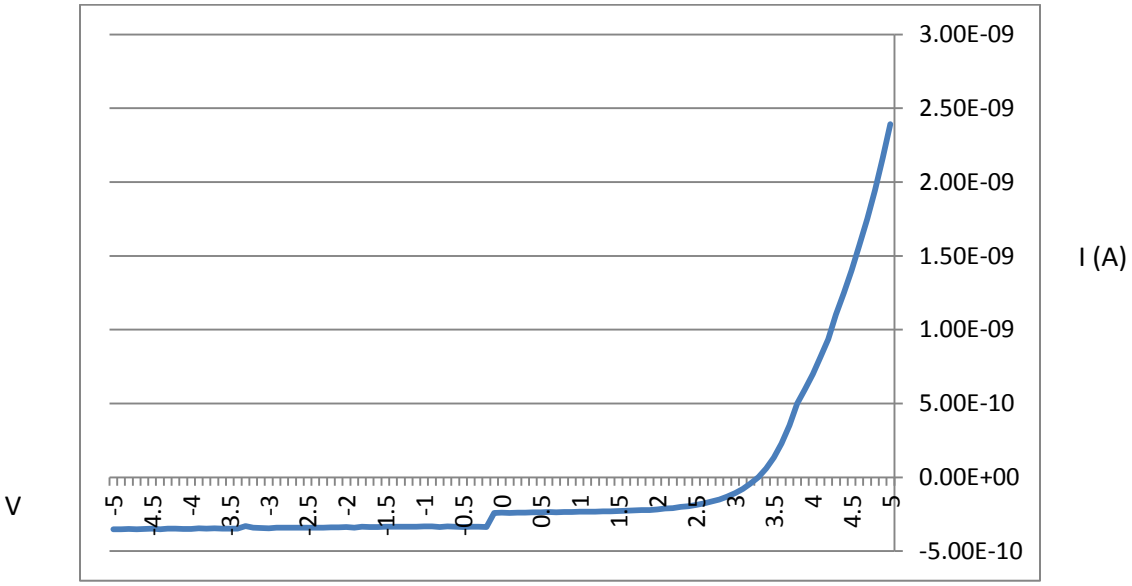

Figure 4.1.0: High resistance leads to minimal currents or emission in a photodetector confirmed to work (with ~1 mA currents) in isolation, now bearing an independently tested OLED design

of apparent good quality. The resistance is highly nonlinear, far beyond the sum of the two devices in series.

4.2 Explanations

When viewing unexpectedly low currents from a photodetector, one trivial possibility to eliminate is remnant oxide resulting in windows that have been incompletely opened atop the mesas. A very thin layer of oxide will not be detectable by profilometer or inspection by microscope, but can still have an appreciable effect. As stated previously, over-etching by wet or dry methods can ensure that no oxide remains, ensuring that low currents do not arise as a consequence of this fabrication error; however, extensive over-etching, particularly with non-selective dry methods (RIE, etc.) will damage the top layer of the photodetector. This can contribute to leakage currents that increase the value of the dark current, reducing the photodetector's signal-to-noise ratio.

If remnant oxide can be eliminated as an issue, the problem of low detector currents may then trace to surface passivation; improper passivation may introduce a massive resistance in devices, and is a more likely explanation for the above figure, which was over-etched to completely clear the oxide window. At the surface of InGaAs or InP surface recombination of carriers can occur to reduce the device's current; treatment with ammonium sulfide is the general method used. One significant complication in passivation is the possibility of volatility in the treatment; even if passivation is done well it may naturally degrade due to exposure to air, moisture and light, and so by the time a substrate is brought to vacuum for deposition the treatment may have degraded to the point of being ineffectual across a significant area of the device. The deposition setup used in these experiments could not bring a sample to vacuum for

deposition swiftly (needing time to mount the sample, and several pump/evacuation cycles to first enter a nitrogen chamber, before entering the thermal deposition chamber to receive the OLED), making this a serious and persistent problem reasonable to suspect. Efforts to make a more enduring passivation treatment to survive the necessary wait must be wary of the risk of damaging the device surface with chemicals or ions, which is especially problematic when the top layers are very thin (the same problem that cautions extensive over-etching to remove remnant oxide). A heavily damaged top surface will similarly permit leakage currents, increasing the dark current and harming the signal-to-noise ratio of the photodetector (and the eventual upconverter).

Dangling bonds at the top of the device structure are the sites of surface recombination, the mechanism that is to be reduced by surface passivation to minimize loss of carriers; Ag and Al layers have their own passivation problems which are addressed with in-chamber deposition of thin layers that eliminate these dangling bonds, MoO_3 and LiF respectively. Given the brightness and stability of glass-based OLEDs exploiting these techniques it is evident that surface passivation has been well-achieved on those interfaces; the InGaAs/OLED interface, however, does not have an in-chamber passivation process in these fluorescent OLED experiments, making surface recombination a relevant problem. Section 4.4 outlines an alternative passivation layer for Al, Al oxide, which has also been investigated by some researchers interested in passivating InGaAs surfaces; this would then constitute an in-chamber no-delay passivation strategy that can approach the success observed for hole injection from Ag and electron injection from Al.

In addition to interface issues, the steps on the surface of a photodetector introduce additional complications that can prevent an OLED from precisely matching its on-glass

performance. The experiments conducted on glass are on a near-ideal flat surface, and the topography of an insulation border, and a mesa etched into the photodetector wafer, with steps ranging from hundreds of nanometers to in excess of 1 micron, has the potential to produce a zone of incomplete contact where the organic layers fail to adhere to the surface. Besides introducing potential breaks in the electrical current across the xy plane, such a step may also disconnect the thinnest layers inside the OLED itself, risking a break in the z direction as the OLED is contorted over the photodetector substrate during deposition. The thinnest layer in OLED designs considered here is the ~1 nm of LiF used to enhance electron injection from Al into Alq_3; if this layer is interrupted in any region of the OLED by rough topography injection will be reduced (along with responsivity of the detector and emission of the OLED). Figure 4.2.0 illustrates the difference between probing directly upon the window and on the window boarder of an HPT photodetector bearing a trial OLED, signifying an increase in resistance caused by some form of disconnection. While a thicker cathode may reduce the influence of such a step, this also compromises light extraction.

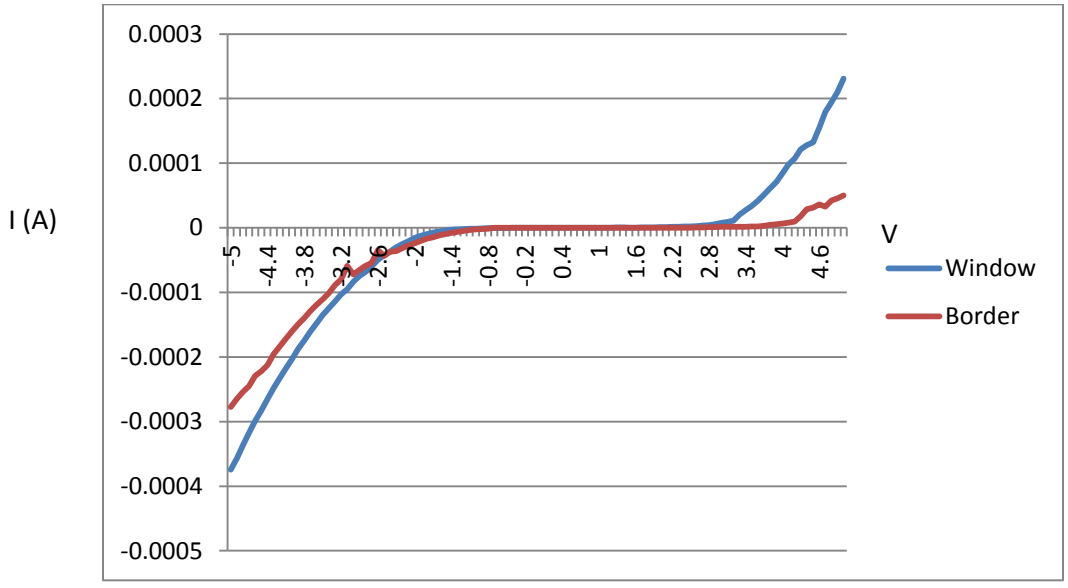

Figure 4.2.0: Topographic disconnection caused by the border step of silicon oxide.

4.3 High Voltage Fluorescent OLEDs

To account for the increase in resistance caused by improper passivation of the InGaAs prior to OLED deposition due to chamber-pumping delays and volatility, the upconverter can be tested at higher biases to induce a sufficiently high current through the OLED section of the device, achieving the necessary bias in that subsection to observe luminescence and upconversion of NIR light. Testing should be streamlined to be done rapidly; it is also important to estimate the extent of the device's aging by conducting identical measurements at the beginning and end of the series of climbing NIR powers, establishing an appropriate baseline which cannot be trusted to be flat.

Figure 4.3.0 illustrates the photocurrent response of an HPT detector tested below 20 V with and without a fluorescent OLED deposited above, illustrating the justification for biasing into this voltage range. The mA photocurrent response established upon the bare photodetector is reduced to a μA response when an OLED is grown on the same photodetector, despite an increase in NIR exposure, indicating that a high resistance impedes delivery of holes to the OLED to ensure practical luminosity. The reduced with-OLED photocurrent begins to increase in a practical range above 20 V.

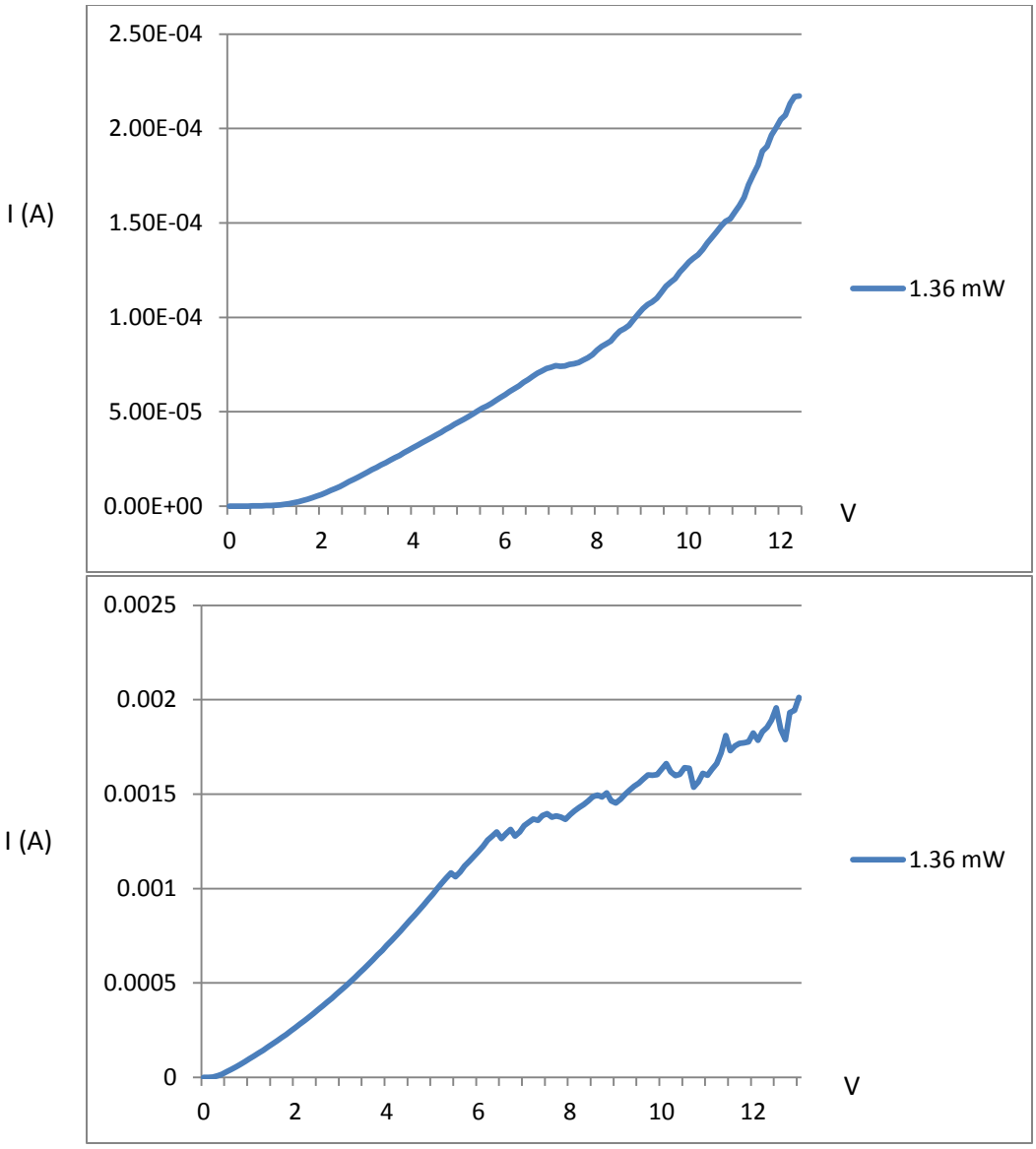

Figure 4.3.0: Photocurrent of bare photodetector (above) and photodetector with fluorescent OLED (below). The reduced photocurrent indicates a significant increase in resistance, likely the consequence of failed surface passivation.

User error becomes more likely if testing is required to be rapid, however, and time and concentration must be spent on focusing a CCD camera upon the OLED to properly establish a luminescence reading. Testing must be done in a dark room to eliminate false positive signals,

and multiple tests should be conducted to account for variation in focus upon the OLED target, minimizing the influence of outlying values. A large number of scans can be considered together to establish the NIR upconversion; the measurements are also considered in chronological order to demonstrate the deterioration of the OLED by electrical aging.

The ultimate (W/W) efficiency of initial upconverters were extremely low, however, the likely consequence of carrier recombination at the photodetector/OLED interface caused by degraded surface passivation. Contrasting with previous upconversion devices founded on similar detectors and OLED designs, which achieved 1.77 percent ultimate efficiency by wafer bonding and in excess of 100 percent by combining an Au mirror with an HPT, the importance of good passivation enduring until the time of deposition is underlined severely: by accounting for device area and converting the luminosity measurements to W/steridian, and calculating for an emissive hemisphere above the device, it can be determined that the peak upconversion efficiency observed in an initial device is no greater than 0.0017 percent. Despite some loss as a consequence of an Au mirror being unworkable in this experiment, the bulk of the inequality (with ~90 thousand times less green light emitted) is thought to be attributable to carrier recombination losses. Poor light extraction in the absence of a refractive-indexed layer (abandoned to ensure probing of the cathode) reduces brightness further.

The weaknesses of a fluorescent OLED are also demonstrated by the impractical dimness of the OLED. The removal of Au from the upconverter design eliminates the Au/NPB interface, which has a conveniently low injection barrier, adding resistance on top of surface recombination to starve the OLED of carriers from the photodetector. The high bias demanded from this high current has also handicapped the stability of the OLED, limiting the number of measurements

that can be taken per device, and limiting the relevance of comparing values that have been extracted from the device at different times.

A chronological luminosity plot (Figure 4.3.1) demonstrates the swift aging of the OLED as it is tested at an elevated bias, with local inconsistencies in the trend tracing to measurements taken at different biases. In the improved characterization setup more than a hundred measurements were taken, in contrast to the paltry fifteen pairs considered in the earlier upconverter.

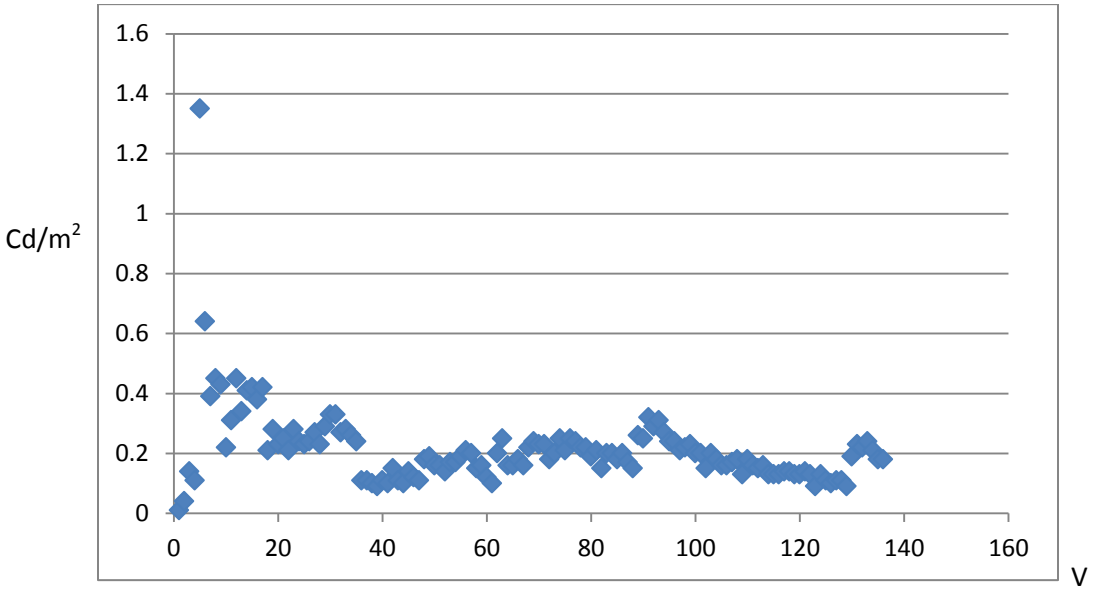

Figure 4.3.1: Chronological luminosity plot of an HPT-based upconverter, demonstrating electrical aging. Rapid aging forbids an initial high luminosity from being repeated.

Not taking aging into account, the average upconversion measurement extracted from this experiment matched the results of the earlier trial: 0.048 Cd/m^2. This value recurred despite swifter measurements and marginally brighter OLED in contrast to the previous experiments.

The highest upconversion results extracted from the device were measured immediately, before electrical aging could affect the device, luminescing about 0.33 Cd/m^2 in response to

about 1.79 mW of NIR exposure (Figure 4.3.2). This still only converts to an ultimate efficiency of about 0.0047 percent, measured once, and the more reliable average upconversion efficiency determined from all measurements is approximately 0.0013 percent as a consequence of electrical aging.

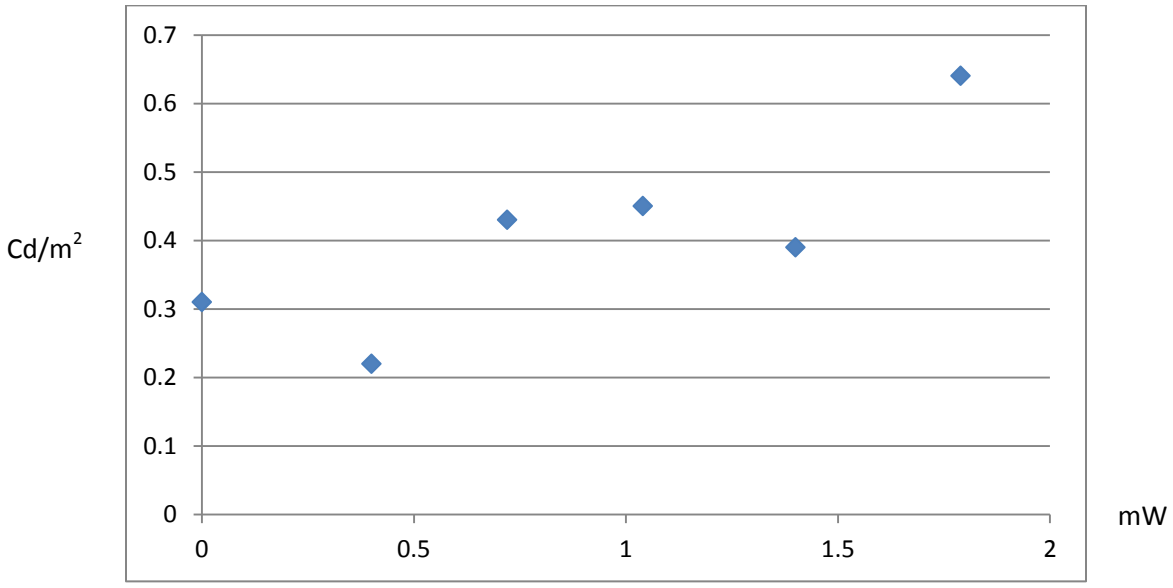

Figure 4.3.2: Peak upconversion performance of an HPT-based upconverter, prior to significant electrical aging.

The high bias used to extract luminescence from these OLEDs necessitates the higher consumption of electrical power by the entire upconverter system. The probability of sparking and electrical shorting between device components is also increased by deploying such voltages. Thicker OLED devices could demonstrate greater stability against aging mechanisms affecting the bulk of organic layers, but many important aging mechanisms operate at material interfaces in OLEDs; the increased thickness of devices also increases global device resistance, potentially demanding greater bias. It is ultimately not possible to neglect the significance of surface passivation in combining an OLED with a photodetector, despite good independent performance

of both devices. The deposition setup must be considered to ensure that organic layers can be deposited upon the photodetector swiftly after the passivation treatment, which will otherwise be erased by volatility, the likely problem here.

4.4 Phosphorescent OLED Upconverter

Fluorescent OLEDs have an inherent limitation in their internal quantum efficiency due to the spin property of the electron, which yields four possible exciton combinations with only one state, the singlet, being capable of fluorescent light emission. This keeps the maximum attainable internal quantum efficiency of such devices at 25 percent, as the other three exciton combinations (75 percent of the excitons produced) are denied emission by conservation of spin angular momentum. Phosphorescent OLEDs permit the recovery of these triplets by converting some of them into singlets by intersystem crossing, made possible by the presence of a heavier element bound within the organic molecules. Recognizing that the fluorescent OLEDs grown on the photodetectors cannot approach the luminosity of their on-glass counterparts with an incomplete surface passivation and an incomplete understanding of surface passivation volatility and failure, a phosphorescent OLED was grown on the photodetector in a subsequent experiment. This trial indeed demonstrated superior luminosity to the fluorescent OLED counterparts, with confirmed upconversion of infrared light. The experiment featured three devices, bearing the same OLED atop a bare photodetector cell, and two Al mirrors of 50 nm and 70 nm.

Figure 4.4.0 presents the phosphorescent OLED structure deposited on the HPT photodetector. AlO_2 in a thin layer serves the purpose of passivating Al in the mirrored devices, serving a role analogous to the MoO_3 used previously to passivate Ag anodes during the

fluorescent OLED trials on glass; the thin layer modifies the work function of the anode metal to produce a smaller hole injection barrier. Aluminum oxides have also been explored in passivation treatments for InGaAs/InP substrates[39], presenting an in-chamber passivation treatment here that is followed by OLED treatment with minimal delay and no oxygen/moisture exposure. The phosphorescent OLED structure follows as in the diagram. Material choice, doping concentration and dimensions were selected under the recommendation of accomplished practitioners more familiar with phosphorescent OLED deposition and performance, who are listed in the Acknowledgements section. Full chemical names are listed in the Abbreviations section.

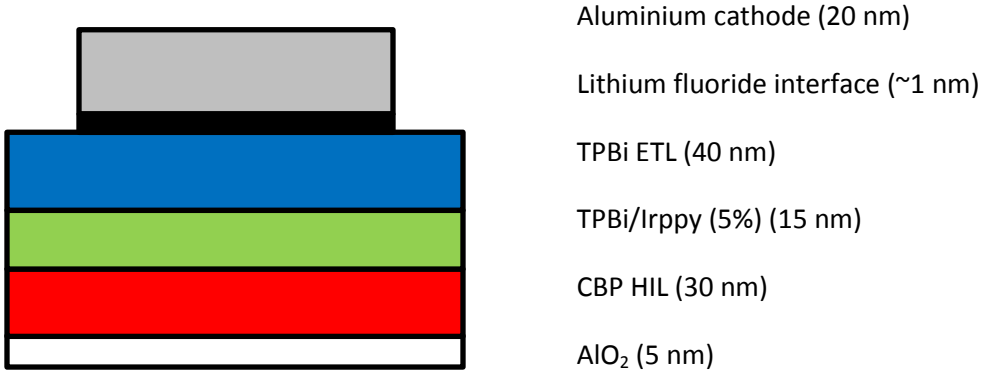

Figure 4.4.0: Phosphorescent OLED structure.

In the above device the Irppy dopant bears iridium, a heavy element able to conduct intersystem crossing to convert excitons in the triplet state into the useable singlet state. The OLED lacks an antireflection coating, as with the fluorescent OLED devices, to conduct probing properly (and for the purposes of a more meaningful comparison with the previous fluorescent OLED upconverters). In these experiments the same photodetectors receive the OLED designs,

which are tested and then removed for deposition of subsequent OLEDs. Imperfections in this cleaning process and their consequences are discussed in section 3.2.2. Figure 4.4.1 presents a scatterplot of luminosities vs. voltages acquired at different exposures of NIR light upon the mirror-free upconverter device; as before, such plots do not account for aging and the chronological order of measurements, confounding some comparisons.

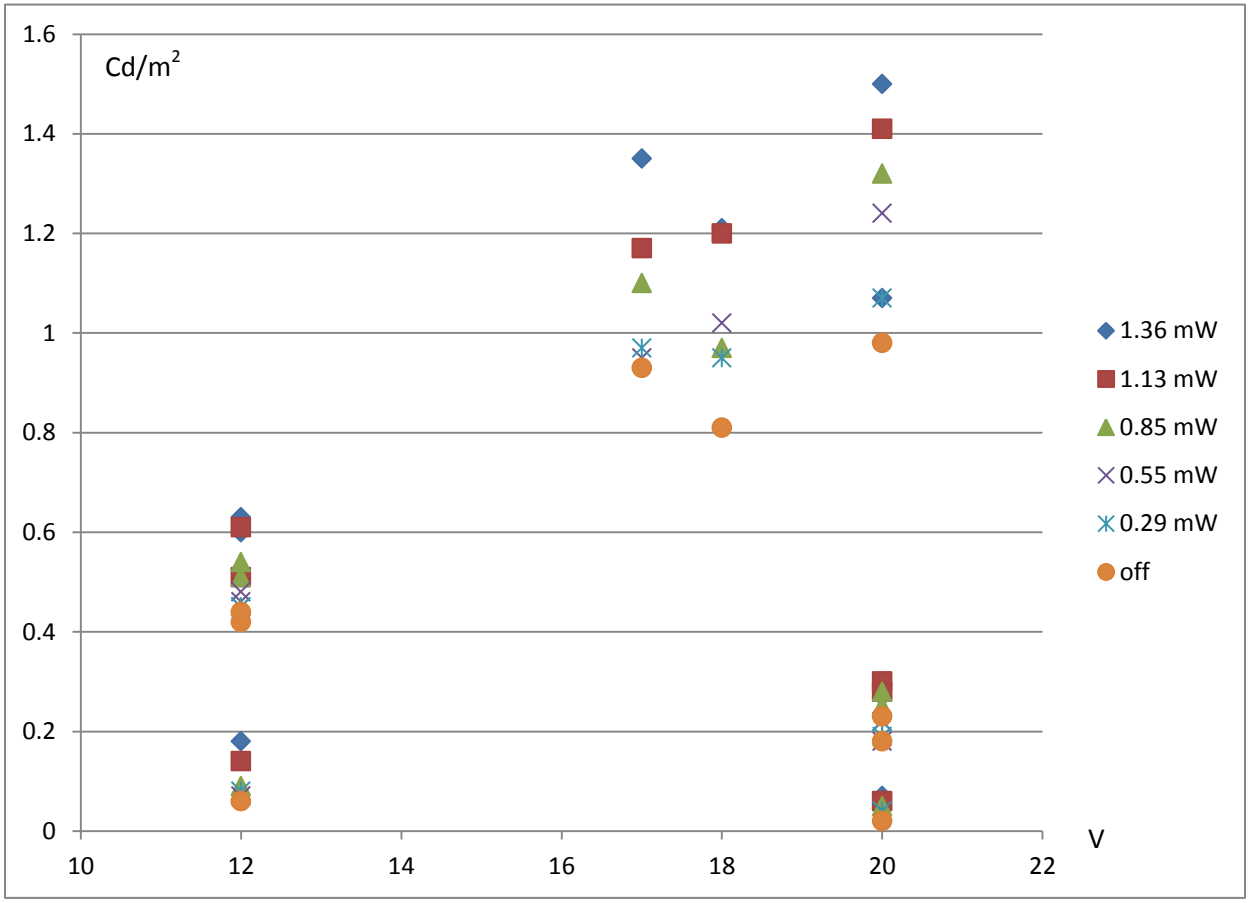

Figure 4.4.1: Luminosity of the phosphorescent OLED on an HPT photodetector, demonstrating superior upconversion in response to increasing NIR exposure in a lower voltage range than the previous fluorescent devices.

This trial yielded the most significant upconversion response of any device; as with previous devices aging occurred to deteriorate the luminosity of the OLED, such that initial measurements were brightest and not repeatable. Figure 4.4.2 presents three sets of data points, each set collected quickly to minimize the effect of aging between data points, demonstrating the peak, mean and aged performance of the mirror-free upconverter.

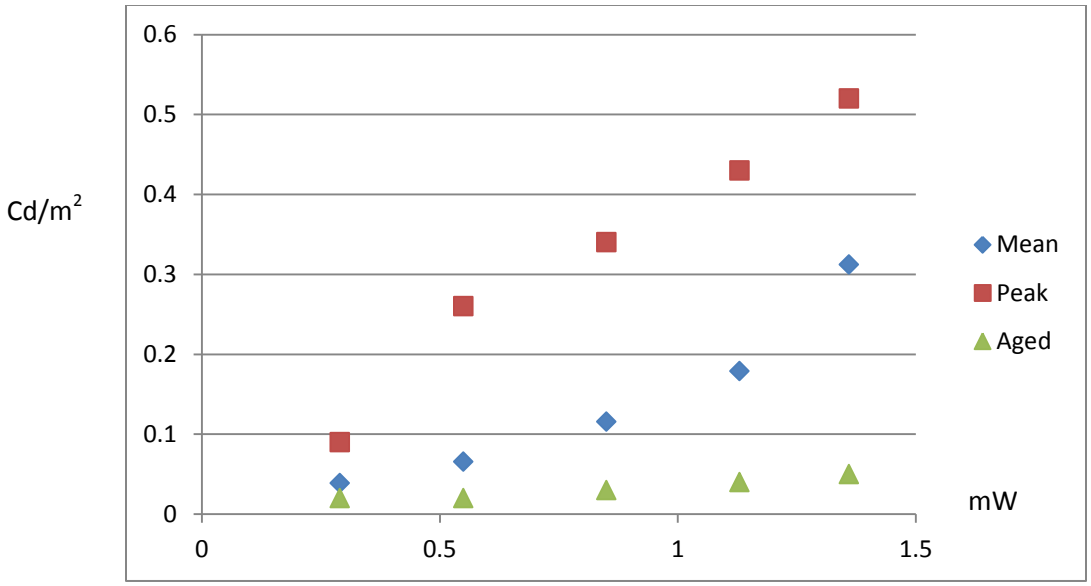

Figure 4.4.2: Phosphorescent OLED luminosity response to increasing NIR power, with peak performance measured at the beginning of characterization. Upconversion deteriorates as the device ages rapidly during testing.

The strongest upconversion response measured is 0.52 Cd/m^2 in response to 1.36 mW/cm^2 NIR infrared light. This still points to a very low ultimate (W/W) device efficiency of 0.00391 percent. Severe non-idealities at work in this device were apparent – emission was observed to not come from the entire photodetector cell, but from a fraction (<10 percent) of the total cell area, reducing the luminosity considerably, and also compromising the accurate delivery of NIR power to the upconversion site given the limitations of the alignment system

used here. This phenomena points to a continuing challenge to understand and improve hole injection at the photodetector/organic interface, a challenge thought to be primarily the work of surface passivation issues; apart from this, topographic disconnection of the thinnest layers in the OLED, particularly the ~1 nm LiF layer used to modify the work function of the Al cathode, is suspected to be significant even with the reduced thickness of the silicon oxide insulation layer and the use of a wet etch to produce a slope in place of a step. This suspicion arises from the observation that the partial cell emission observed occurred at the window edge.

Average results from this trial indicate a mean upconversion responsivity reduced by this partial-cell emission problem, which was more severe than in the case of fluorescent OLED trials. These differing areas of functional cell make a straightforward quantitative comparison of fluorescent and phosphorescent-based upconverters inappropriate; however, that the phosphorescent OLED device outperformed the fluorescent OLED device despite having a smaller area of emission does indicate the successful realization of superior brightness tracing to the intersystem crossing permitted by phosphorescent materials and the liberation of exciton triplets into singlets. The inclusion of phosphorescent OLED designs on future upconverters, especially upconverters retaining the Au mirror and all its advantages, is therefore recommended.

The two other devices receiving phosphorescent OLEDs, each bearing an Al mirror, demonstrated the same shorting problem that discouraged the use of Ag mirrors. Al was attempted as a substitute mirror material over the first substitute of Ag for Au by the properties of its oxide. Aluminum oxide is an insulator, whereas silver oxide is a conductor; it was therefore supposed that any oxide intruding into cracks, pores, or similar imperfections in the silicon oxide passivation layer, or into damage in the top layer of the photodetector itself, would not present so severe a shorting risk if it were an oxide of aluminum in contrast to silver. Nevertheless, both Al

mirrors shorted, demonstrating a more severe problem with metal intrusion into flaws in these device layers. In the absence of a reflective mirror to simultaneously improve photodetector adsorption and OLED light extraction (apart from other subtractions, such as the absence of an anti-reflection coating due to probing concerns, and the absence of good InGaAs surface passivation due to pumping delays and treatment volatility) the devices cannot approach the performance of previous upconverters established in literature. The rejection of Au as a mirror material, and as a material from which hole injection proceeds at a reasonable bias into conventional fluorescent OLED materials (NPB), presents a significant challenge to these upconverters founded on alternative material choices.

Chapter 5

5.0 Conclusions

In this work upconversion was demonstrated in the absence of a Au mirror; other reductions to the upconverter exercised here include the absence of an anti-reflection coating to assist in OLED light extraction so as to achieve a connection while probing devices, and the restriction to fluorescent OLED materials for most of the experiments discussed. The most important result to consider is the success of an Ag-based anode for the fluorescent OLED design used on previous upconversion devices when tested on glass, and the great reduction in performance, or outright failure, of that same design when it is replicated with all due precision on a functional photodetector to create an upconverter. Large area deposition of Ag as a mirror layer prior to OLED deposition consistently resorted in electrical shorts, indicating sufficiently frequent flaws in the silicon oxide insulation layer and/or the photodetector's top layer to permit the intrusion of metal and shorting of the device, and/or shorting caused by incomplete cleaning. Even a mirror suspected to circumvent the shorting issue with a more suitable oxide, based on Al, demonstrated the same shorting issue. Only mirror-free upconverter devices could be repeatedly made and confirmed to operate.

The most obvious change from moving an OLED from a glass test substrate to the photodetector is the introduction of complex topography, and the risk of topographic disconnection incurred by device features on the order of hundreds of nanometers, particularly upon layers of minimal thickness on the order of a single nanometer. The partial performance of photodetector cells covered in both fluorescent and phosphorescent OLEDs, and the location of

functional fractions within the cell (predominantly in contact with the border) suggests that the window border does compromise OLED performance by some form of disconnection.

However, considering within the functional area of the photodetector cells, it is finally concluded that surface passivation remains the obstacle most compromising to efficient light emission in response to NIR exposure. The recombination of carriers at the interface starves a large fraction of the photocurrent, incurring a significant resistance observed here (lowering currents from mA to micro-amps, and lower). This interfacial resistance demands testing at higher voltages to achieve sufficient bias across the OLED layers of the device, introducing potential faults due to shorting, greater power consumption, and challenges in safely collecting experimental data with test equipment designed to forbid overly high voltages.

The failure of surface passivation shown here is traced to significant limitations in the deposition equipment which interfere with the normal operation of preparing an InGaAs surface for additional layers. Passivation was successfully achieved on Ag by deposition of a MoO_3 layer followed immediately by deposition of the OLED layers, producing a bright Ag-anode fluorescent OLED on glass. Passivation of Al with LiF was also confirmed to be quite operational. Done in vacuum, without delay, these passivation treatments were unambiguously superior to attempts to passivate the photodetector surface by chemical bath followed by delays and exposure to air and moisture before OLED deposition. An analogous in-chamber passivation layer for InGaAs, as achieved with Al and Ag, would be a significant improvement; a thin layer of aluminum oxide was used to passivate Al in the phosphorescent OLED trial, but this material has also been considered for passivating InGaAs as well. Done in-chamber without delay, success as with Ag and Al is more reasonable.

Other areas demanding improvement including the testing apparatus, particularly the delivery of NIR power to the device so as to produce clear and unambiguous photocurrents and upconverter luminosities consistently between measurements and several devices. A NIR source with a raw power of about 50 mW/cm^2 experiences significant absorption as it passes through the photodetector substrate, such that no device in this thesis is exposed properly (from below) beyond 2 mW/cm^2. Operating in this low power regime, there were challenges in observing the expected behavior of the photodetectors with photocurrents needing repeated verification to distinguish from noise. An effort to increase power delivery with lenses, to create a more intense beam, is workable but produces a smaller beam which is more difficult to accurately position upon the photodetector and the upconverter, producing greater exposure diversity due to inconsistent xy positioning.

The requirements of probing demanded the absence of an antireflection layer atop the cathode structure; this allowed for probing both on and off the window to evaluate the relevance of the topographic step in disconnecting the cathode and affecting the performance of the OLED, but also reduces the light extracted from the OLED. Shutter masks shaped for the particular device would allow full and partial coverage of photodetector cells with such an index-matching layer, observing its enhancement while still permitting probing inside the window. It is also noteworthy that all HPT devices fabricated and used to make upconverters presented in this thesis were pnp-doped devices, injecting holes into the OLED and having their light extraction limited by the transparency of the cathode; transparent anodes for OLED devices, founded on Ag and ITO, are an active area of research, and might provide superior light extraction in npn-doped upconverter structures with an inverted OLED structure, though the anode would still be subject to the topographic disconnection problem.

References

[1] R. Jedicke, A. Morbidelli; T. Spahr, J.M. Petit, Bottke, F. William, "Earth and space-based NEO survey simulations: prospects for achieving the Spaceguard Goal", *Icarus*, vol. 161, iss. 1, pp. 17-33, Jan. 2003.

[2] E.O. Gracheva, N.T. Ingolia, Y.M. Kelly, J.F. Cordero-Morales, G. Hollopeter, A T. Chesler, E.E. Sánchez, J.C. Perez, J.S. Weissman, D. Julius, "Molecular basis of infrared detection by snakes," *Nature*, 464 (7291):1006-1011, April 2010.

[3] A. Rogalski, "History of infrared detectors," *Opto-Electron. Rev.*, vol. 20, no. 3, pp. 279-308, 2012.

[4] C. Kittel, "Introduction to Solid State Physics, 6th Ed.," New York, John Wiley, pg. 185, 1986.

[5] T.P. Pearsall, R.W. Hopson, "Growth and characterization of lattice-matched epitaxial films of $Ga_xIn_{1-x}As$/InP by liquid-phase epitaxy," *J. Electron. Mat.*, vol. 7, iss. 1, pp.133-146, 1978.

[6] W.T. Tsang, "Semiconductors and Semimetals, Volume 22," Academic Press, June 3, 1985.

[7] J. Sparkes, "Semiconductor Devices, 2nd Edition". CRC Press, July 1994.

[8] H. Schneider, H.C. Liu, "Quantum Well Infrared Photodetectors: Physics and Applications," Springer, October 2006.

[9] M. Davis, M. Greiner, "Indium antimonide large-format detector arrays," *Optical Engineering*, vol. 50, iss. 6, April 2011.

[10] J. Chen, "Hybrid Organic/Inorganic Optical Upconversion Devices," Doctoral Thesis, 2011.

[11] P. Franken, A. Hill, C. Peters, G. Weinreich, "Generation of Optical Harmonics," *Physical Review Letters*, 7 (4): 118, 1961.

[12] H.C. Liu, J. Li, Z.R. Wasilewski, M. Buchanan, "Integrated quantum well intersubband photodetector and light emitting diode," *Electronics Letters*, vol. 31, pp. 832-833, 1995.

[13] D. Ban, H. Luo, H.C. Liu, A.J. Springthorpe, Z.R. Wasilewski, "1.5 μm optical up-conversion: wafer fusion and related issues," *Infrared Spaceborne Remote Sensing XII*, *Proceedings of SPIE*, vol. 5543, 2004.

[14] W. Helfrich, W. Schneider, "Recombination Radiation in Anthracene Crystals," *Physical Review Letters*, 14 (7): 229, 1965.

[15] H. Aziz, Z.D. Popovic, N.X. Hu, A.M. Hor, G. Xu, "Degradation mechanism of small molecule-based organic light emitting devices," *Science*, 283(5409):1900-1902, 1999.

[16] H. Aziz, Y. Luo, G. Xu, Z.D. Popovic, "Improving the stability of organic light-emitting devices by using a thin Mg anode buffer layer," *Applied Physics Letters*, 89(10), 103515, 2006.

[17] J. Chen, D. Ban, M.G. Helander, Z.H. Lu, P. Poole, "Near-Infrared Inorganic/Organic Optical Upconverter with an External Power Efficiency of >100%," *Advanced Materials*, 22, 4900-4904, 2010.

[18] J. Chen, J. Tao, D. Ban, M.G. Helander, Z. Wang, J. Qiu, Z. Lu, "Hybrid Organic/Inorganic Optical Up-Converter for Pixel-less Near-Infrared Imaging," *Advanced Materials*, 24, 3138-3142, 2012.

[19] J. Tao, "Pixel-less and Pixel-lated Inorganic/Organic Hybrid Infrared Imaging Upconversion Devices," Masters Thesis, 2012.

[20] P. Frigeri, L. Seravalli, G. Trevisi, S. Franchi, "Comprehensive Semiconductor Science and Technology: Volume 3: Materials, Preparation and Properties," Elsevier B.V., 2011.

[21] A.R. Barron, "Chemistry of Electronic Materials," Connexions, Rice University, Houston, Texas, 2012.

[22] A. Bonecutter, A. Schoenborn, M.A. Thomas, “Cleanroom Processing Modules: Cleanroom processing information: Institute for Electronics and Nanotechnology,” Georgia Institute of Technology, 2013.

[23] J. E. O’Reilly, “Fluorescence experiments with quinine,” *J. Chem. Educ.*, 52 (9), pg. 610, 1975.

[24] “Giga-to-Nanoelectronics Centre – Lab Equipment”. University of Waterloo.

[25] “EMD Performance Materials (North America): Electronic Materials: Products: AZ Photoresists,” Emanuel Merck Darmstadt, 2014.

[26] G. Williams, R. Barber, “Giga-to-Nanoelectronics Centre – Operating Policies and Procedures,” University of Waterloo, 2011.

[27] M.K. Rathi, G. Tsvid, A.A. Khandekar, J.C. Shin, D. Botez, T.F. Kuech, “Passivation of Interfacial States for GaAs- and InGaAs/InP-Based Regrown Nanostructures,” *Journal of Electronic Materials*, 2009.

[28] D. Sheela, N. DasGupta, “Optimization of surface passivation for InGaAs/InP pin photodetectors using ammonium sulfide,” *Semiconductor Science and Technology*, vol. 23, no. 3, 2008.

[29] “Newport: Optical Mirror Selection Guide,” Newport Corporation, 2015.

[30] H. Lin, J.S. Yu, W. Zhang, “Investigation of top-emitting OLEDs using molybdenum oxide as anode buffer layer,” *Optoelectronics Letters*, vol. 8, no. 3, May 2012.

[31] H. Peng, X. Zhu, J. Sun, Z. Xie, S. Xie, M. Wong, H. Kwok, “Efficient organic light emitting diode using semitransparent silver as anode,” *Applied Physics Letters*, vol. 87, iss. 17, 2005.

[32] C. Chen, "Top-emitting organic light-emitting devices using surface-modified Ag anode," *Applied Physics Letters*, vol. 83, iss. 25, 2003.

[33] J. Li, J. Huang, Y. Yang, "Improved hole-injection contact for top-emitting polymeric diodes," *Applied Physics Letters*, vol. 90, iss. 17, 2007.

[34] G.E. Jabbour, B. Kippelen, N.R. Armstrong, N. Peyghambarian, "Aluminum based cathode structure for enhanced electron injection in electroluminescent organic devices," *Applied Physics Letters*, vol. 73, iss. 9, 1998.

[35] J. Shinar, "Organic Light-Emitting Devices: A Survey," Springer Science & Business Media, 2004.

[36] J.E. Knox, M.D. Halls, H.P. Hratchian, H.B Schlegel, "Chemical failure modes of AlQ3-based OLEDs: Alq3 hydrolysis," *Physical Chemistry Chemical Physics*, iss. 12, 2006.

[37] A. Buckley, "Organic Light-Emitting Diodes (OLEDs): Materials, Devices and Applications," Elsevier, 2013.

[38] S. Reineke, K. Walzer, K. Leo, "Triplet-exciton quenching in organic phosphorescent light-emitting diodes with Ir-based emitters," *Phys. Rev. B*, 75, 125328, March 2007.

[39] M.L. Huang, Y.C. Chang, C.H. Chang, Y.J. Lee, P. Change, J. Kwo, T.B. Wu, M. Hong, "Surface passivation of III-V compound semiconductors using atomic-layer-deposition-grown Al_2O_3," *Applied Physics Letters*, vol. 87, iss. 25, 2005.

Glossary:

Intersystem crossing: Triplet transition into a singlet state, occurring in phosphorescence due to a strong spin-orbit interaction.

Lattice-matching: agreement between lattice parameters of crystals to ensure growth without significant strain.

Non-linear optical materials: materials featuring significantly non-parabolic energy potentials for electrons, permitting such phenomena as Second Harmonic Generation.

Piranha etch: explosive and corrosive solution (combining sulphuric acid, hydrogen peroxide and water) used to etch such materials as InGaAs. Must be neutralized after use.

Quencher: Material allowing for non-radiative loss of excitons, reducing fluorescence.

Second Harmonic Generation: emission of a photon with doubled energies from two absorbed photons, occurring in non-linear optical materials.

Spin-orbit interaction: Phenomena in heavy-atom molecules favoring a change in spin, which can liberate triplet excitons by intersystem crossing.

Tapetum lucidum: reflective coating in the eyes of many nocturnal animals; Latin for 'bright tapestry.'

Thermography: imaging of temperature differences (producing thermograms).

Upconversion: production of output light of greater energy than the input light